

# Prostaglandin E<sub>2</sub> regulates senescence and post-senescence neoplastic escape in primary human keratinocytes

Elise Srour<sup>1,\*</sup>, Nathalie Martin<sup>1,\*</sup>, Claire Drullion<sup>1,\*</sup>, Clémentine De Schutter<sup>1</sup>, Joëlle Giroud<sup>1</sup>, Adrien Pioger<sup>1</sup>, Julie Deslé<sup>1</sup>, Laure Saas<sup>1</sup>, Joe Nassour<sup>5</sup>, Julien Théry<sup>2</sup>, Gauthier Decanter<sup>3</sup>, Nicolas Penel<sup>2,4</sup>, Chantal Vercamer<sup>1</sup>, Clara Salazar-Cardozo<sup>1</sup>, Corinne Abbadie<sup>1</sup>, Olivier Pluquet<sup>1</sup>

<sup>1</sup>CNRS, Inserm, CHU Lille, Institut Pasteur de Lille, UMR9020 – U1277 – CANTHER - Cancer Heterogeneity, Plasticity and Resistance to Therapies, University of Lille, Lille F-59000, France

<sup>2</sup>Direction of Clinical Research and Innovation, Oscar Lambret Center, Lille, France

<sup>3</sup>Department of Surgical, Oscar Lambret Center, Lille, France

<sup>4</sup>CHU Lille, ULR 2694 - Metrics: Evaluation des Technologies de Santé et des Pratiques Médicales, University of Lille, Lille, France

<sup>5</sup>Department of Biochemistry and Molecular Genetics, University of Colorado School of Medicine, Aurora, CO 80045, USA

\*Equal contribution

**Correspondence to:** Olivier Pluquet; **email:** [olivier.pluquet@ibl.cnrs.fr](mailto:olivier.pluquet@ibl.cnrs.fr)

**Keywords:** PTGS2, prostaglandins, EP receptors, senescence, neoplastic transformation, keratinocyte

**Received:** November 15, 2023

**Accepted:** October 15, 2024

**Published:** November 18, 2024

**Copyright:** © 2024 Srour et al. This is an open access article distributed under the terms of the [Creative Commons Attribution License](https://creativecommons.org/licenses/by/4.0/) (CC BY 4.0), which permits unrestricted use, distribution, and reproduction in any medium, provided the original author and source are credited.

## ABSTRACT

Aging of the epidermis partially occurs as a consequence of epidermal cell senescence, a non-proliferative state in which cells remain metabolically active and acquire changes in their secretome. We previously reported that senescent normal human epidermal keratinocytes (NHEKs) have two opposite outcomes: either cell death by excess of autophagic activity or escape from senescence to give rise to post-senescence neoplastic emerging (PSNE) cells. In this study, we investigated the role of PTGS2, the inducible enzyme of the prostaglandin biosynthesis pathway, in the onset of NHEK senescence and in the switch from senescence to pre-transformation. We provide evidence that the PTGS2/PGE<sub>2</sub>/EP4 pathway plays a critical role in NHEK senescence as well as in senescence escape. We show that treating proliferating NHEKs with prostaglandin E<sub>2</sub> (PGE<sub>2</sub>) or with an agonist of one of its receptors, EP4, induced the establishment of the senescent phenotype, according to several markers including the senescence-associated β-galactosidase activity. Conversely, treating already senescent NHEKs with an antagonist of EP4, or knocking-down PTGS2 by siRNA resulted in the decrease of the percentage of senescence-associated β-galactosidase-positive cells. We also demonstrate that the PSNE frequency was significantly decreased upon PTGS2 silencing by siRNA, pharmacological PTGS2 inhibition, or treatment by an EP4 antagonist, while on the contrary treatments with PGE<sub>2</sub> or EP4 agonist increased the PSNE frequency. These results indicate that the PTGS2/PGE<sub>2</sub>/EP4 pathway is required to induce and maintain the senescent phenotype of NHEKs, and that PGE<sub>2</sub> level is a potential determinant of the initial steps of the age-related oncogenic process.

## INTRODUCTION

The skin epidermis has a high rate of cell turnover to continuously reconstruct itself and to ensure the

protection of the body. This protection can be compromised during physiological aging and photo-aging due to UV overexposure, both conditions associated with skin inflammation and accumulation of

senescent cells [1–4]. Keratinocyte senescence may impair epidermis functions leading to pathological conditions including the development of non-melanoma skin carcinoma which are the human cancer with the highest incidence [5].

Senescence is a cellular state known as an anti-tumor barrier, that can be induced by different stimuli including shortening of telomeres leading to replicative senescence (RS) or various endogenous or exogenous genotoxic agents leading to stress-induced premature senescence (SIPS) [6, 7]. The cell cycle arrest of senescent cells often depends on the activation of two main pathways, p53/p21<sup>WAF1</sup> and/or p16<sup>INK4</sup>/pRb, in an interconnected or independent manner [8]. Regarding RS, high p21<sup>WAF1</sup> expression was found during the final 2–3 passages before the onset of the senescent plateau, but its expression does not persist, suggesting that it is not essential for maintaining the senescence phenotype [9, 10]. p16<sup>INK4A</sup> seems to take the relay, with an expression increased later [9, 10], but robustly maintained along the senescence plateau (see for review [11]). Regarding SIPS, the cell cycle arrest can be ensured through activation of the p53/p21<sup>WAF1</sup> or the p16<sup>INK4A</sup>/Rb pathway, or through both (reviewed in [12–14]). Senescent cells display deep molecular changes, including alterations in metabolic, epigenetic, and gene expression programs [12, 14], leading to an increase in senescence-associated  $\beta$ -galactosidase (SA- $\beta$ -Gal) activity and to profound changes in the senescence-associated secretory phenotype (SASP) which is enriched in pro-inflammatory cytokines, growth factors and remodeling enzymes of the extracellular matrix [7, 14–16]. Growing evidence showed that the SASP can play a critical role in tumorigenesis [17].

Epidermal keratinocytes display at senescence most of the characteristics of an adaptive response to stress [12]. Using a model of *in vitro* cultured Normal Human Epidermal Keratinocytes (NHEKs) and samples of human skin from donors at different ages, we have shown that senescence in epidermal keratinocytes occurs without any significant telomere shortening, but in response to an increase in intracellular concentration of reactive oxygen species (ROS). This oxidative stress leads to a cell cycle arrest mediated by the sole p16/Rb pathway. It also results in a high macroautophagic activity, associated with an increase in Beclin1 and a decrease in BCL2 expressions, leading to cell death without activation of the apoptotic pathway [18–20]. If most of senescent NHEKs in culture die by an excess of autophagy, a very few of them nevertheless remain alive and are permissive to the generation of neoplastic post-senescent cells [12]. Indeed, we have shown that a few rare senescent NHEKs can spontaneously and systematically escape from the senescent state. They re-enter cell cycle via a process we

called PSNE (Post-Senescence Neoplastic Escape) which leads to clonal populations of daughter cells having acquired characteristics similar to those observed during the early stages of tumor initiation [21–23]. More importantly, when xenografted in *nude* mice, these PSNE cells developed in disseminated skin lesions such as hyperplasias and small non-melanoma skin carcinomas, providing evidence of their tumorigenic potential [22, 23].

The biosynthesis of prostaglandins (PGs) begins with the release of arachidonic acid from phospholipid membranes by the enzyme phospholipase A2. Arachidonic acid is then metabolized by the prostaglandin endoperoxide synthases PTGS1 and PTGS2 (also called cyclooxygenases COX1 and COX2) to form prostaglandin H<sub>2</sub> (PGH<sub>2</sub>). PGH<sub>2</sub> is the precursor of all series of prostaglandins and thromboxanes (TX). It is the substrate of different tissue-specifically expressed PG and TX synthases to generate a range of prostanoids including PGE<sub>2</sub>, PGD<sub>2</sub>, PGI<sub>2</sub>, PGF<sub>2</sub> $\alpha$ , and TXA<sub>2</sub> [24]. Prostanoids exert their biological effects in a paracrine, autocrine, or intracrine manner through binding with prostanoid receptors. Prostanoid receptors control various biological functions not only through their sensitivity to the prostaglandins themselves, but also through the different receptor isoforms and the diversity of coupled G-proteins [25]. The active site of PTGSs is inhibited by most of non-steroidal anti-inflammatory drugs (NSAIDs). PTGS1 has been defined as a constitutive and ubiquitous enzyme that generates PGs controlling physiological homeostasis including platelet function and renal blood flow [26] [27]). In contrast, PTGS2 is an inducible enzyme whose expression is increased by various stimuli including growth factors, cytokines, and chemokines [26]. PTGS2 is involved in various processes leading to inflammation [28, 29], and plays a causal role in cancer [30, 31].

Several studies pointed the role of PTGS2 in senescence and aging of the dermis: (i) PTGS2 expression is increased in human aged skin, including fibroblasts of the dermis, compared to normal young skin [32, 33] and, in accordance, NS398, a selective PTGS2 inhibitor, has been shown to reduce skin aging in mice [34]; (ii) PTGS2 takes part in replicative senescence of *in vitro* cultured normal human dermal fibroblasts (NHDFs) [35], and NS398 also reduced this function [36]. The mechanisms were not fully dissected. We have shown that PGE<sub>2</sub> acts on NHDF senescence via the pool of intracellular EP3 receptors [37]. Recently, PTGS2 was suggested to regulate the SASP composition through PGE<sub>2</sub> [38].

Although PTGS enzymes were shown to contribute to the early stages of keratinocyte differentiation [39], nothing is known on the role of PTGSs in epidermis aging and keratinocyte senescence. We therefore investigated the

functional involvement of the PTGS2 pathway in senescence of NHEKs and its impact on post-senescence neoplastic escape. By using functional approaches (including RNA interference, pharmacological inhibitors of PTGS2 activity, and agonists and antagonists of EPs), we identified the PTGS2/PGE<sub>2</sub>/EP4 pathway as a driver in both the establishment of senescence in NHEKs, and the promotion of the very initial phases of neoplastic transformation by senescence escape in a context of aging.

## RESULTS

### PTGS2 is upregulated in normal human epidermal keratinocytes during *in vitro* senescence and skin aging

The present study was performed using six different donors of NHEKs, from different sex, age and ethnicity group. As we already published [18–21, 40, 41], in standard culture conditions, these NHEKs enter senescence in 1 to 3 weeks and 10 to 15 cumulative population doublings according to the cell donor (Supplementary Figure 1A). At the senescence plateau, NHEKs display SA-β-Gal activity (Supplementary Figure 1B), cell spreading (Supplementary Figure 1C), and increase in cell size and granularity as observed by flow cytometry (Supplementary Figure 1D).

We investigated the PTGS2 expression at the mRNA and protein levels in exponentially growing, pre-senescent and senescent NHEKs. RT-qPCR analyses show that PTGS2 mRNA levels are increased at senescence compared to exponentially growth phase (Figure 1A). This up-regulation was confirmed by Western Blot (Figure 1B) and was correlated to an increase in the protein levels of p16<sup>INK4a</sup>, MnSOD, a marker of redox control that we previously showed as upregulated in senescent NHEKs [20], and to a decrease in PCNA, a marker of proliferation, and in GPX4, an antioxidant marker whose expression is down-regulated at senescence [42]. By immunofluorescence, the endogenous PTGS2 was barely detectable in growing NHEKs while it was highly expressed in 100% of senescent NHEKs identified by the presence of XRCC1 foci, as marker of DNA single-strand breaks (SSBs) (Figure 1C). To assess the *in vivo* relevance of these results, we analyzed PTGS2 protein levels in skin sections of young (18–40 years old) and old (>55 years old) healthy subjects by immunofluorescence. In skin sections of young people, PTGS2 protein levels were not detected in the dermis and hardly any in the epidermis. In skin section of old people, PTGS2 expression was significantly increased, mainly in the epidermis, in the basal layer containing proliferating keratinocytes, and in the upper layers containing terminally differentiated

keratinocytes (Figure 1D). The staining intensity measure showed a statistically significant difference between the two groups ( $P < 0.01$ ) (Figure 1D). These data are in agreement with PTGS2 immunohistological staining found in aged skin epidermis by Habib et al. [32] and confirm that an induction of PTGS2 expression is associated with senescence and aging of human epidermal keratinocytes.

### PTGS2 controls the establishment and maintenance of some senescence markers in NHEKs

To determine whether PTGS2 is causally involved in the onset of senescence in NHEKs, we first cultured proliferating NHEKs (at 8.8 population doublings) in the presence of 5 or 10 μM NS398, an inhibitor of PTGS2 activity. We then followed the appearance of senescence criteria. After seven days, NS398 partly prevented the establishment of the senescence growth plateau, and the appearance of the SA-β-Gal activity (Figure 2A), suggesting that PTGS2 was necessary for the occurrence of NHEK senescence. We then silenced PTGS2 expression by RNA interference or inhibited its activity with two different pharmacological inhibitors (NS398 and rofecoxib) in already senescent NHEKs to assay whether PTGS2 contributes to the maintenance of senescence. The efficacy of PTGS2 silencing was checked by Western-blotting experiments which indicated that the expression of PTGS2 at the protein level was highly repressed after four days post-transfection (Figure 2B). At this same point, PTGS2 silencing significantly reduced the percentage of SA-β-Gal-positive cells (Figure 2B). Similar results were obtained with the highest concentrations of PTGS2 inhibitors (Figure 2C). We also examined the consequences of PTGS2 inhibition on the SASP. We first analysed the composition of conditioned media (CM) from proliferating and senescent NHEKs using a cytokine array. We identified different cytokines/chemokines that were significantly over-secreted by senescent NHEKs compared to proliferating ones, such as GM-CSF (=CSF2), G-CSF (=CSF3), IL10, CXCL1, CCL5 (Supplementary Figure 2). Surprisingly, IL-6, IL-8, or TNFα were not overdetected in senescent NHEKs. They are nevertheless considered as major components of the SASP, but most often established using models fibroblasts at replicative senescence, confirming that SASP composition is influenced by the cell-type and the senescence inducer [16]. We then examined whether the secretion of GM-CSF and G-CSF was dependent on PTGS2 activity. For that, we collected the CM from proliferating or senescent NHEKs exposed or not to NS398 and determined the concentration of GM-CSF and G-CSF by ELISA. The results indicated that PTGS2 activity was required for the secretion of GM-CSF and G-CSF (Figure 2D).

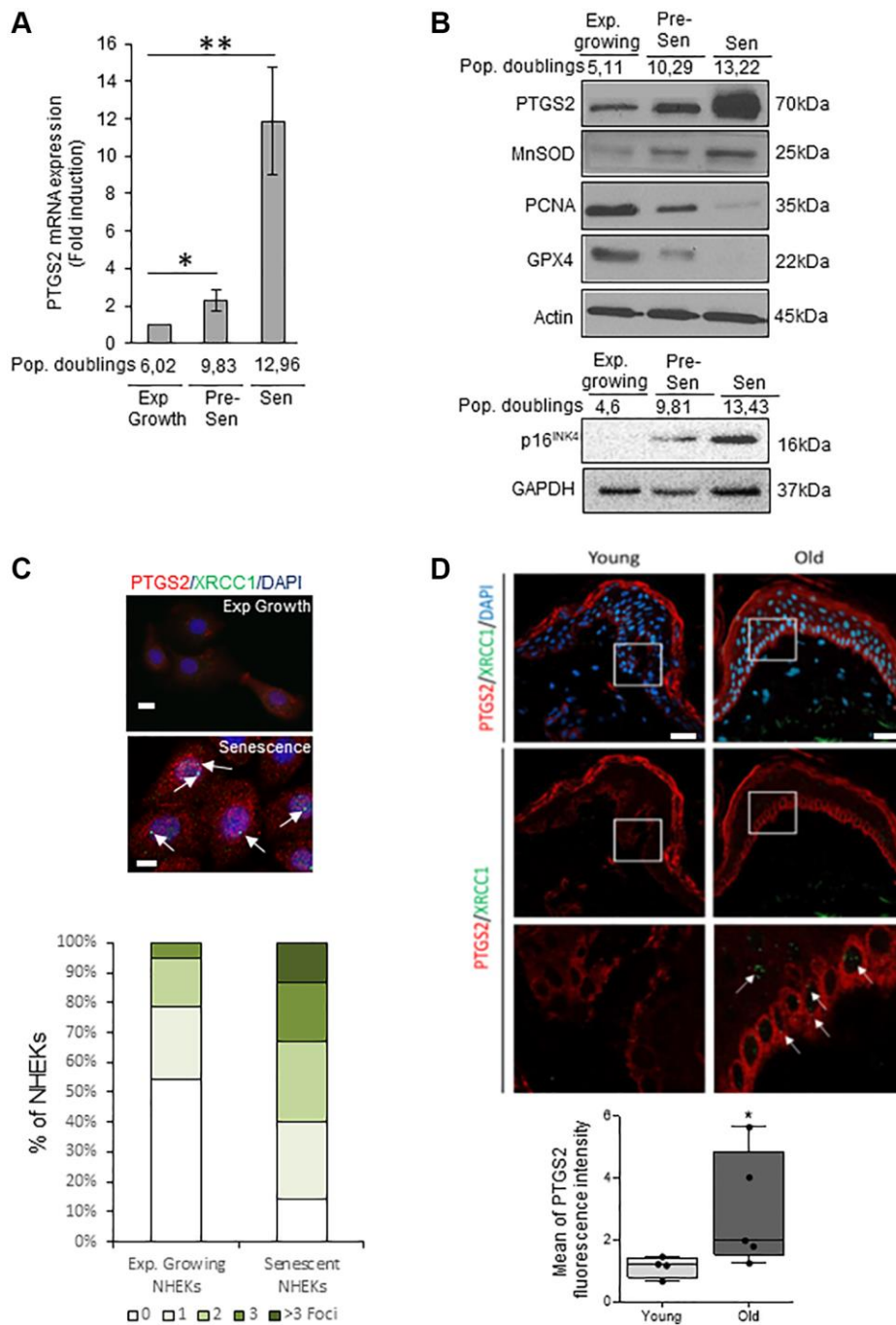


**Figure 1. PTGS2 is up-regulated during NHEK *in vitro* senescence and skin aging.** (A) The mRNA levels of PTGS2 were measured by RT-qPCR in extracts from exponentially growing, pre-senescent and senescent NHEKs (donor 4F0315). PTGS2 levels were normalized to EAR levels. The bars represent the mean  $\pm$ SD ( $p < 0.05$ ;  $**p < 0.01$ ). (B) PTGS2, MnSOD, PCNA, and GPX4 protein levels were evaluated by Western Blot in extracts from exponentially growing, pre-senescent and senescent NHEKs (upper panel: donor 4F0315; lower panel: donor K40FH1). The gel was equicharged with extracts from an equal number of cells. The equicharge was verified *a posteriori* by detecting the levels of actin and GAPDH. (C) Exponentially growing and senescent NHEKs (donor K3MC1) were fixed and processed for immunofluorescence detection of endogenous proteins PTGS2 (red) and XRCC1 (green). Cell nuclei were detected by DAPI staining (blue). Upper panel: Representative confocal photomicrographs of PTGS2 immunostaining and XRCC1 foci (white arrows). Bars represent 20  $\mu$ m. Lower panel: XRCC1 foci were quantified. Measures were done in five independent microscopic fields for a total of at least 100 cells for each condition. The histogram represents the average  $\pm$  S.D. of five contents. Results are representative of at least two independent experiments. (D) Immunofluorescence detection of PTGS2 (red) performed in sections of skin samples from human young ( $n = 4$ ) and old ( $n = 5$ ) healthy subjects (see Material and Method) ( $*p < 0.05$ ). Cell nuclei were detected by DAPI staining (blue). Upper panel: representative confocal microscopy images for epidermis and dermis of a young (37 years old) and an elderly donor (85 years old). The squares delimit the below images at higher magnification. Bars represent 40  $\mu$ m. Lower panel: scatter dot plots indicating the mean fluorescence intensity in

cells of the basal layer. A minimum of 25 cells per sample were selected individually in order to obtain a mean fluorescence for each donor. The horizontal black lines denote median values and the boxes the interquartile ranges (IQR). Vertical lines extend from max value (upper quartile + 1.5\*IQR) to min value (lower quartile - 1.5\*IQR).

All together, these results suggest that PTGS2 is involved in the establishment and maintenance of senescence in NHEKs.

### PTGS2 does not contribute to NHEK senescence by producing an oxidative stress

In previous studies, we demonstrated that *in vitro* and *in vivo* senescence of human epidermal keratinocytes

results from an increase in ROS concentration [18, 19, 40]. However, we still have not identified the origin of this oxidative stress. Since the PTGS2 catalytic activity of conversion of arachidonic aci into PGH<sub>2</sub> generates a side-production of ROS, mainly O<sub>2</sub><sup>-</sup> and OH [43–45], we made the hypothesis that PTGS2 could contribute to NHEK senescence by this mechanism. We therefore first determined the level of ROS generated by the PTGS2 activity in NHEKs by silencing PTGS2 or by

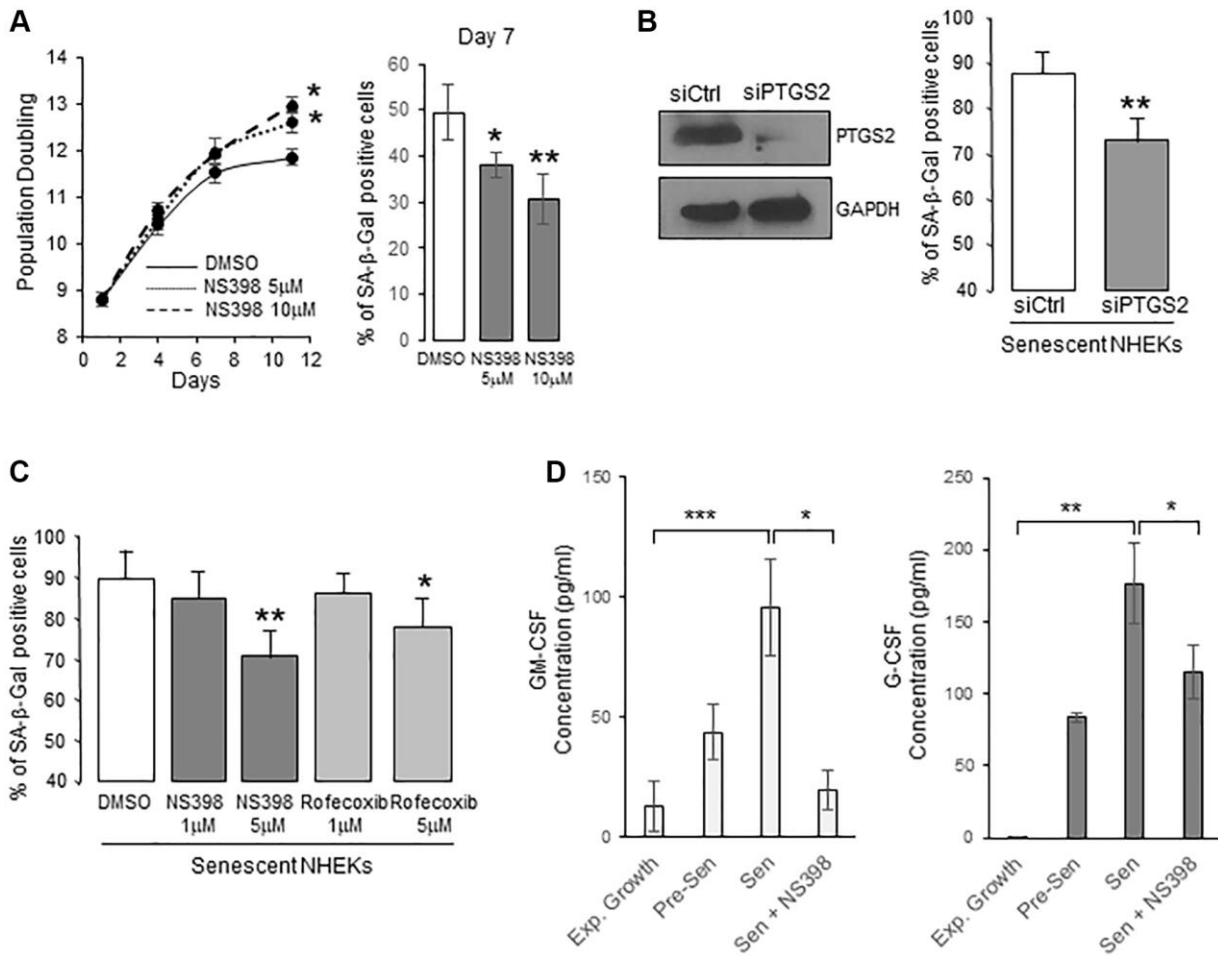


**Figure 2. PTGS2 induces and maintains NHEK senescence.** (A) NHEKs (donor 4F0315) were treated with NS398 at 5 or 10 μM or DMSO every 48 h. Left panel: During the treatment, cells were passaged when reaching 70% confluence, counted, and the number of population doublings was calculated (see Methods). The experiment was performed in triplicate, each point representing the mean of three counts. Significant differences between DMSO control and 5 or 10 μM NS398 treatment are indicated. Right panel: Senescent NHEKs were treated as in (A), then, a SA-β-Gal assay was performed seven days post-treatments. (B) Senescent NHEKs (donor K23FC1) were transfected with a pool of 4 siRNAs targeting PTGS2, or with non-target siRNAs. Left panel: Evaluation of the efficacy of the siRNAs by Western Blot. GAPDH was used as a loading control. Right panel: Four days after transfection, a SA-β-Gal assay was performed. The bars represent the mean ±SD of three counts of blue cells (\*\**p* < 0.01). (C) Senescent NHEKs (donor K23FC1) were treated with NS398 or rofecoxib at the indicated concentrations for four days. Then, a SA-β-Gal assay was performed. The bars represent the mean ±SD of three counts of blue cells (\**p* < 0.05; \*\**p* < 0.01). (D) ELISA assays for measuring the amounts of GM-CSF and G-CSF in the conditioned media (secreted) of exponentially growing, pre-senescent and senescent NHEKs (donor K40FH1) treated or not with NS398 (5 μM) for 16 hrs. Measures were performed in triplicate. The bars represent the mean ± SD of three counts. Significant differences are indicated with asterisks with \**p* < 0.05; \*\**p* < 0.01; \*\*\**p* < 0.001.

using the selective PTGS2 inhibitors NS398 and rofecoxib. ROS concentrations were measured by fluorimetry using H<sub>2</sub>DCFDA, a cell permeant probe which fluoresces upon oxidation. As already shown [19], the ROS levels highly increased in senescent NHEKs compared to proliferating ones. However, neither the pharmacological inhibition (Supplementary Figure 3A), nor the silencing of PTGS2 (Supplementary Figure 3B) altered the overall ROS production in proliferating or senescent NHEKs (compared to their respective controls). This indicates that the ROS-generating activity of PTGS2 does not significantly contribute to the overall ROS production involved in the induction and maintenance of NHEK senescence.

### **PTGS2 contributes to NHEK senescence through the production of PGE<sub>2</sub>**

We then examined whether PTGE<sub>2</sub> could control NHEK senescence through its PG production. The main PGs produced by normal human keratinocytes are PGE<sub>2</sub>, PGF<sub>2</sub> $\alpha$  and PGD<sub>2</sub> [46]. We therefore first investigated by RTqPCR the gene expression level of PGE synthases (PGES) downstream of PTGSs: PTGES1 and PTGES2 (producing PGE<sub>2</sub>), PGFS (producing PGF<sub>2</sub> $\alpha$ ), PGIS (producing PGI<sub>2</sub>), PTGDS (producing PGD<sub>2</sub>), and TXAS1 (producing TXA<sub>2</sub>), in both growing and senescent NHEKs. As expected for human keratinocytes [46], PGIS and TXAS1 expressions were not detected. Surprisingly, PTGES2 expression was not detected as well. Only the expression of PTGES1 and PGFS significantly increased at senescence compared to exponentially growth phase (Figure 3A). Based on these results, we measured the amount of PGE<sub>2</sub>, PGD<sub>2</sub>, and PGF<sub>2</sub> $\alpha$  secreted by growing and senescent NHEKs. Both the secretion of PGE<sub>2</sub> and PGF<sub>2</sub> increased in senescent compared to growing NHEKs. As controls, these elevated levels were abolished in the presence of NS398 (Figure 3B). PGD<sub>2</sub> was not detected, in accordance with the very low level of PTGDS expression.

We therefore focussed on the investigation of the role of PGE<sub>2</sub> and PGF<sub>2</sub> on NHEK senescence. For that, we silenced PTGES1 and PGFS expression by RNA interference and, after having verified siRNA efficiencies (Supplementary Figure 4), we determined the effects on senescence markers. After 4 days post-transfection, only PTGES1 silencing significantly reduced the percentage of SA- $\beta$ -Gal-positive cells (Figure 3C). We also collected the CM from senescent NHEKs treated or not with siRNA and determined by ELISA the levels of GM-CSF, G-CSF and IL-10. The results indicated that only PTGES1 was able to significantly modulate the secretion of IL-10 and G-CSF, but not of GM-CSF (Figure 3D). It is worth to

note that adding exogenous PGE<sub>2</sub> partially rescued IL-10 production in senescent NHEKs knocked-down for PTGS1 (Supplementary Figure 5).

Then, to evaluate the potential role of PGE<sub>2</sub> to induce NHEK senescence through an autocrine, paracrine or intracrine mechanism, we treated cultures of proliferating NHEKs with increasing concentrations of exogenous PGE<sub>2</sub> and examined whether this could induce premature senescence. Given the poor stability of prostaglandins in aqueous solutions, we added PGE<sub>2</sub> to the culture medium four times a day. We observed a statistically significant increase in the number of SA- $\beta$ -Gal-positive cells at 1 and 10  $\mu$ M of PGE<sub>2</sub> (Figure 3E), as well as a decrease in cell proliferation at 10  $\mu$ M of PGE<sub>2</sub> (Figure 3F). All together, these data indicate that the PTGS2/PTGES1/PGE<sub>2</sub> pathway is causally involved in the onset and maintenance of senescence in NHEKs.

### **EP4 activation triggers senescence in NHEKs**

In order to determine through the activation of which EP receptor PGE<sub>2</sub> induces senescence in NHEKs, we first evaluated by RT-PCR the expression of the different EPs. Surprisingly, among the four EPs, we detected only EP1 and EP4 mRNAs in NHEKs, in contrast to NHDFs in which the four EPs were expressed (Figure 4A). We next analyzed EP1 and EP4 protein levels in skin sections of young and old healthy subjects. Immunofluorescence against EP1 and EP4 proteins showed that their expressions were significantly increased in the epidermis of old people compared to young ones (Figure 4B).

To test the involvement of a signalisation through EP1 and/or EP4 in the induction of NHEK senescence, we used specific cell-permeant pharmacological agonists/antagonists of each EP (Figure 4C). We first treated exponentially growing NHEKs with agonists of EP1 (Iloprost) and EP4 (L-902,688 or Rivenprost) and found that only one EP4 agonist (L-902,688) increased the number of SA- $\beta$ -Gal-positive cells (Figure 4D). We then treated already senescent NHEKs with antagonists of EP1 (AH6809) and EP4 (L-161,982) [47] and found that antagonizing EP4 but not EP1 significantly decreased the number of SA- $\beta$ -Gal-positive cells (Figure 4E). Similarly, only one EP4 agonist (L-902,688) led to an increased production of GM-CSF by proliferating NHEKs (Figure 4F) and only the EP4 antagonist to a decreased release of GM-CSF by already senescent NHEKs (Figure 4G).

These results strongly suggest that the PTGS2/PGE<sub>2</sub>/EP4 pathway is involved in the onset and the maintenance of NHEK senescence.

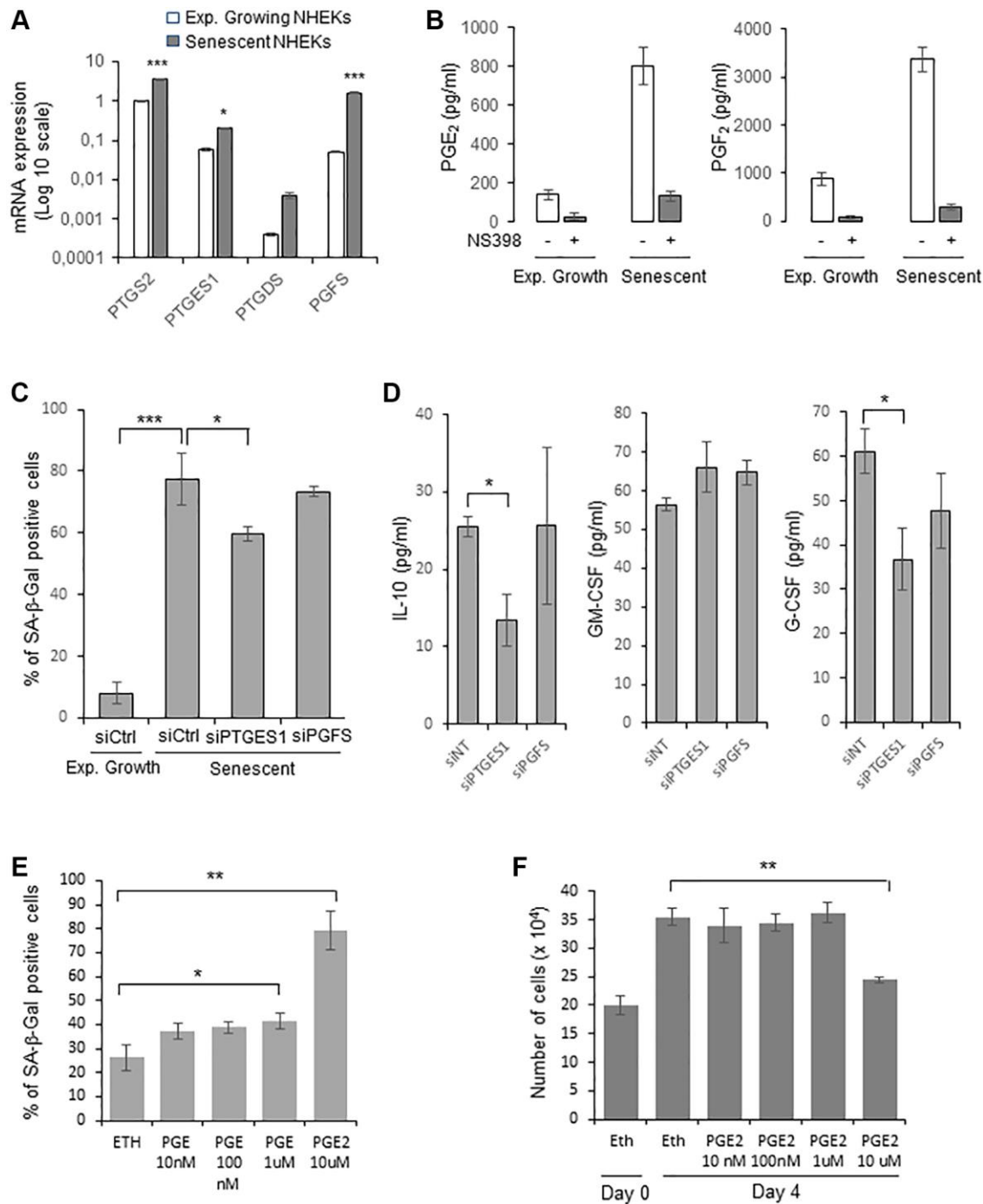


**Figure 3. PGE<sub>2</sub> contributes to the establishment and maintenance of senescence in NHEKs.** (A) PTGS2, PTGES1, PTDGS, and PGFS mRNA levels were measured by RT-qPCR in NHEKs (donor K67FA1) at the exponential growth phase or at the senescence plateau and were normalized to EAR levels. Results are presented in log 10 scale relative to PTGS2 expression in exponentially growing NHEKs (\**p* < 0.05; \*\*\**p* < 0.001). (B) The amount of PGE<sub>2</sub> and PGF<sub>2</sub> in the culture media (secreted) of exponentially growing or senescent NHEKs (donor K67FA1) were measured by a competitive assay (see Material and Methods). Measures were performed in triplicate. The bars represent means ± SD. (C) Senescent NHEKs (donor K40FH1) were transfected with a pool of 4 siRNAs targeting PTGES1 or PGFS, or with non-target siRNAs (siCtrl). Four days after transfection, a SA-β-Gal assay was performed. The bars represent the mean ± SD of three counts (\**p* < 0.05; \*\*\**p* < 0.001). (D) The amounts of IL-10, GM-CSF and G-CSF in the conditioned media (secreted) were measured by ELISA assays in NHEKs (donor K40FH1) treated as in (C). Measures were performed in triplicate. The bars represent the mean ± SD. Significant differences are indicated with asterisks with \**p* < 0.05. (E) Pre-senescent NHEKs (donor K23FC1) were treated or not with 10 nM to 10 μM PGE<sub>2</sub> 4-times a day. The percentage of SA-β-Gal positive cells 4 day after the beginning of the treatment was determined. The bars represent the mean ± SD of three counts (\**p* < 0.05; \*\**p* < 0.01). (F) Pre-senescent NHEKs (donor K23FC1) were treated as in (E), the number of cells was then determined. The bars represent the mean ± SD of three counts (\*\**p* < 0.01).

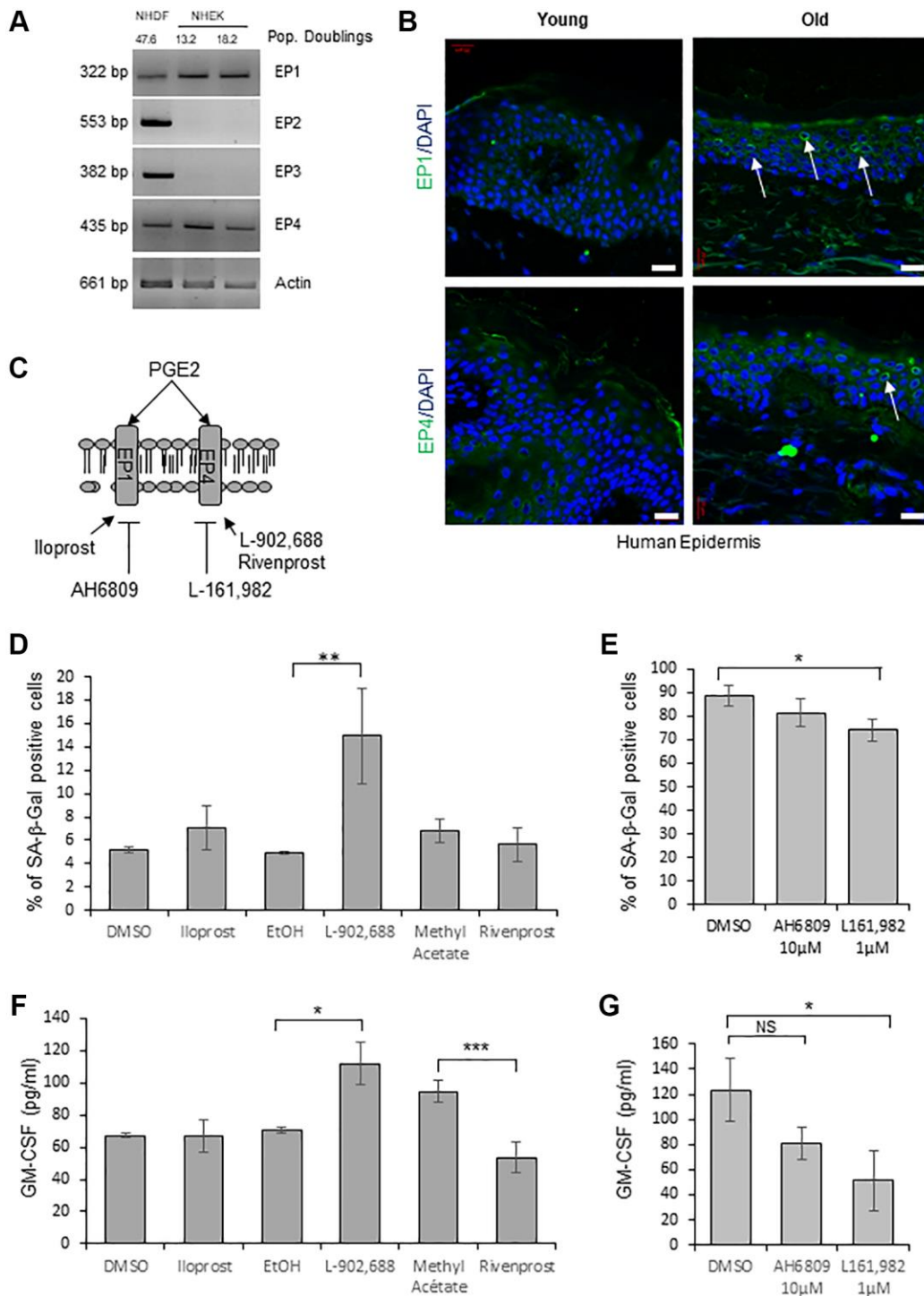


**Figure 4. EP4 receptors mediate senescence of epidermal keratinocytes.** (A) The mRNA levels of EPs were detected by RT-PCR in extracts from exponentially growing and senescent NHEKs (donor 4F0315) and in NHDFs at the replicative senescence plateau. Actin levels were used as control. The number of population doublings for NHDFs and NHEKs are indicated. (B) Immunofluorescence detection of EP1 and EP4 (green) performed in sections of skin samples from human young and old healthy subjects (see Material and Method). Cell nuclei were detected by DAPI staining (blue). Representative confocal microscopy images of the epidermis of a young (37 years old) and an elderly donor (83 years old). Positive staining of EP1 and EP4 (white arrows) are shown. Bars represent 20 μm. (C) Scheme of PGE<sub>2</sub> receptors and their agonists/antagonists used in the following experiments. (D) NHEKs (donor K40FH1) at the exponential growth phase were treated with the EP1 or EP4 agonists (Iloprost, L-902,688 and Rivenprost, respectively at 100 ng/mL, 1 μM and 100 nM) for 4 days. The percentage of SA-β-Gal-positive cells was determined 4 days after the beginning of treatment. SA-β-Gal-positive cells were counted in at least 3 different microscopic fields. The bars represent the mean ± SD of at least 3 counts (\*\**p* < 0.01). (E) Senescent NHEKs (donor K23FC1) were treated with EP1 and EP4 antagonists (AH6809 and L-161,982, respectively at 10 μM and 1 μM). The percentage of SA-β-Gal-positive cells

was determined 4 days after the beginning of treatment. SA- $\beta$ -Gal-positive cells were counted in at least 3 different microscopic fields. The bars represent the mean  $\pm$  SD of at least 3 counts ( $*p < 0.05$ ). (F) NHEKs (donor K40FH1) at the exponential growth phase were treated as in (D), the amounts of GM-CSF in the conditioned media (secreted) were measured by an ELISA assay. Measures were performed in triplicate. The bars represent the mean  $\pm$  SD. Significant differences are indicated with asterisks with  $*p < 0.05$  and  $***p < 0.001$ . (G) NHEKs (donor K40FH1) at the exponential growth phase were treated as in (E), and the amount of GM-CSF in the conditioned media (secreted) was measured by an ELISA assay. Measures were performed in triplicate. The bars represent the mean  $\pm$  SD. Significant differences are indicated with asterisks with  $*p < 0.05$ .

### The PTGS2/PGE<sub>2</sub>/EP4 pathway regulates the post-senescence neoplastic emergence frequency

In previous studies, we had shown that a few senescent NHEKs can spontaneously and systematically escape from the senescent state and re-enter cell cycle at a frequency of  $10^{-2}$  to  $10^{-4}$  to generate a progeny of (pre)neoplastic cells by an unusual asymmetric mitosis mechanism (budding). We named this process “Post senescence neoplastic emergence” (PSNE) [22, 41] (Figure 5A and Supplementary Figure 6). Here, we investigated whether PTGS2 silencing or pharmacological inhibition could alter the process of PSNE. To this end, senescent NHEKs were transfected with siRNAs against PTGS2, plated at low density, and monitored for emergence during up to 6 days. The emergence frequency was quantified by counting the number of PSNE clones per plated senescent cells. Silencing PTGS2 significantly decreased the PSNE frequency (Figure 5B). Similarly, the treatment of senescent NHEKs by non-toxic concentrations of NS398 or rofecoxib significantly decreased the PSNE frequency in a dose-dependent manner (Figure 5C). No cell death was observed in the remaining adherent keratinocytes after siRNA or pharmacological treatments (not shown). Then we wondered whether, on the contrary, an excess of PGE<sub>2</sub> given to senescent NHEKs could favour or not neoplastic evasion. To address this question, senescent NHEKs plated at low density were treated with exogenous PGE<sub>2</sub> (10 and 100 nM) and the emergence frequency was monitored as above. The results show that 100 nM PGE<sub>2</sub> in the culture medium of senescent NHEKs increased the PSNE frequency (Figure 5D). Next, we determined whether the PSNE frequency can be modified in response to EP1/4 activity modulation. We first treated senescent NHEKs with the EP4 agonist L-902,688, but it turned out to be toxic after 4 days of treatment (which was not the case in proliferating NHEKs, see Figure 4D), preventing the determination of the emergence frequency. So, we replaced L-902,688 with another EP4 agonist called Rivenprost, and showed that only Rivenprost, but not the EP1 agonist Iloprost, increased the emergence frequency (Figure 5E). We then wanted to confirm these results by treating senescent NHEKs with the EP1 and EP4 antagonists. Only the EP4 antagonist L-161,982, but not the EP1 antagonist AH6809, treatment significantly reduced the PSNE frequency (Figure 5F).

All these results indicate that the neoplastic senescence escape was controlled, at least in part, by the PTGS2/PGE<sub>2</sub>/EP4 pathway.

## DISCUSSION

Our data indicate that the PTGS2 level and the production of PGE<sub>2</sub> are increased during *in vitro* senescence of NHEKs, as well as during aging of skin epidermal keratinocytes. This hormone production plays a role both in the establishment of the senescence state, in its maintenance, as well as in the escape to generate (pre)neoplastic cells.

We had demonstrated in several previous studies [19] [20] that senescence in epidermal keratinocytes is mainly the consequence of an increase of an endogenous oxidative stress whose origin remained unestablished. By producing ROS [43–45], the catalytic activity of PTGS2 could have been one of these sources of oxidative stress. However, our results demonstrate that it is not the case, since silencing or pharmacologically inhibiting PTGS2 did induce a partial reversal of senescence but without altering total ROS levels. We therefore explored whether PTGS2 contributes to senescence directly through the prostanooids produced by the downstream prostaglandin synthases. Although PGE<sub>2</sub> and PGF<sub>2</sub> were both highly overproduced by senescent NHEKs in consequence of an up-regulation of PTGES1 and PGFS respectively, our results indicate that PGE<sub>2</sub> was the main pro-tanglandin involved in the induction and maintenance of the senescent phenotype, and in senescence escape. PGE<sub>2</sub> mainly acts paracrinally, autocrinally or intracrinally by binding to membrane or intracellular forms of the G protein-coupled receptors EP1, 2, 3 and 4 [48]. Our results indicate that only EP1 and EP4 are expressed in epidermal keratinocytes. Although both of them are slightly up-regulated with *in vitro* senescence or during skin aging, EP4 seems to play the most important role in NHEK senescence induced by PGE<sub>2</sub>. Indeed, inhibiting EP4 using a pharmacological antagonist partly reversed some senescence markers, whereas activating EP4 with an agonist induced a premature senescent phenotype.

These results evidencing the contribution of a PTGS2 dependent-PGE<sub>2</sub> pathway in the senescence of human epidermal keratinocytes are similar to those we

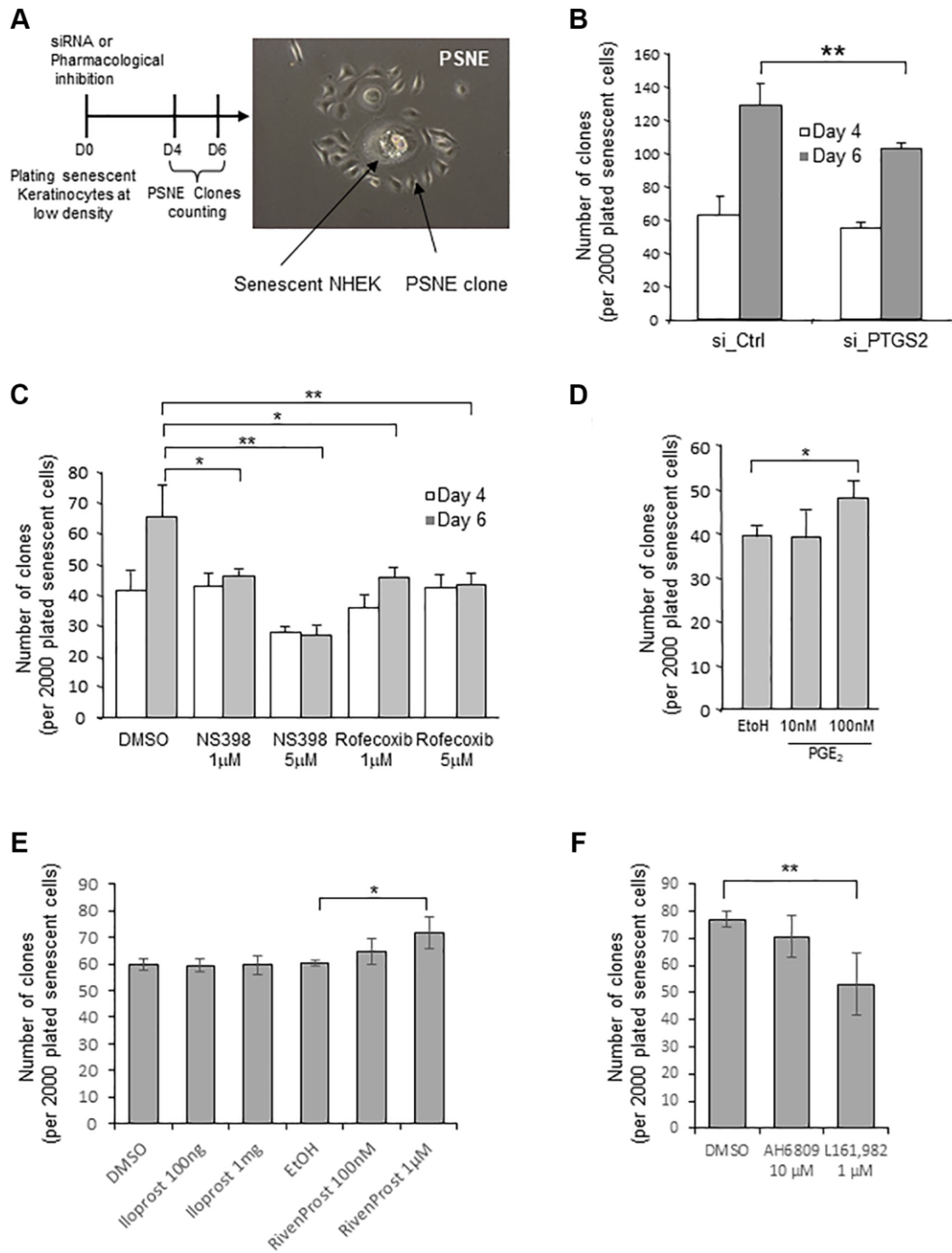


**Figure 5. Loss of PTGS2 activity reduces preneoplastic senescence escape of NHEKs.** (A) Left panel: Scheme depicting the experimental process. Right panel: representative phase contrast microscopy image of what was counted as a clone in the following experiments. (B) Senescent NHEKs (donor K67JA1) were subjected to PTGS2 siRNAs vs. non-target control siRNAs. After four- or six-days post-transfection, emerging clones were manually counted under microscopic examination after fixation and coloration with crystal violet. (C) Senescent NHEKs (donor K23C1) were subjected to PTGS2 pharmacological inhibition by NS398 or Rofecoxib at the indicated concentrations. Four- or six-days post-treatment, emerging clones were manually counted as in B. (D) Senescent NHEKs (donor KNBMC1) were treated or not with 10 or 100 nM PGE<sub>2</sub> 4-times a day. After four days of treatment, the number of emerging clones was counted as in B. (E) Senescent NHEKs (donor K40FH1) were treated with the EP1 or EP4 agonists (Iloprost and Rivenprost at the indicated concentrations). After four days of treatment, the number of emerging clones was counted as in B. (F) Senescent NHEKs (donor K40FH1) were treated with EP1 and EP4 antagonists (AH6809 and L-161,982, respectively at 10 µM and 1 µM). After four days of treatment, the number of emerging clones was counted as in B. In (B–F), the bar chart represents the mean ± SD of the 3 independent measures (\**p* < 0.05; \*\**p* < 0.01). In (B–F), each result is representative from 3 independent experiments, with each experiment corresponding of three or four technical replicates.

previously obtained with human dermal fibroblasts undergoing replicative senescence [37]. Therefore, PGE<sub>2</sub> could be a universal player in senescence, whatever the senescence inducer -oxidative stress in keratinocytes, telomeres shortening in fibroblasts- and whatever the cell type. However, the involved EP receptor type differs in the two contexts, EP3 in fibroblasts *versus* EP4 in keratinocytes. Both are high affinity receptors for PGE<sub>2</sub>, but they transduce the signal through different G-proteins, Gi for EP3 and G<sub>s</sub> for EP4, with a downstream canonical signaling pathway involving the phospholipase C or the PI3K respectively [48].

It is now clearly established that accumulation of senescent cells in tissues and organs [2, 49] plays a causal role in the effects of aging, by limiting the organismal lifespan and increasing the incidence of many age-related disorders and pathologies [50–52]. Interestingly, the inhibition of PTGS2 was shown to extend the life span in *C. Elegans* [53], highlighting the crucial role of PTGS2 in aging. To support this, aging was shown to be associated with a severalfold increase in PTGS expression, production of PGH<sub>2</sub>, and downstream synthesis of active prostanoids [54, 55]. For example, serum from 24-month-old rats showed significant increase of PGE<sub>2</sub>, compared to 6-month-old rats [56]. Similarly, PGE<sub>2</sub> levels from elderly persons were higher than those in young ones [57]. Our present results show that the PTGS2 protein level was higher in the epidermis of elderly subjects than in young ones support and enlarge these data, highlighting a general role for prostaglandins in aging.

To decipher the molecular mechanisms that lead to transformation in a context of aging, we took advantages of our cultured NHEK model. Unlike to NHDFs which are stably and irreversibly cell cycle arrested when they reach an *in vitro* replicative senescence plateau associated with shortened telomeres, NHEKs prematurely enter *in vitro* senescence well before reaching a critical telomere length, because of an increase in endogenous oxidative stress. Again, in contrast to the replicative senescent state of NHDFs, the senescent state of NHEKs is unstable, with the vast majority of cells that die by autophagic programmed cell death, and a very few of them that spontaneously and systematically escape cell death and re-enter in the cell cycle to generate post-senescent cells harbouring preneoplastic and neoplastic markers [18, 22, 21]. Thereby, this model could mimic the physiopathology of the earliest carcinogenesis step and give access to a mechanistic understanding of this step, and not just to the pre-transformed state once established. In previous studies, we had identified several parameters controlling the ability of senescent NHEKs to re-enter cell cycle:

The metabolism of xenobiotics by cytochrome p450 pathway via AKR1C2 and AKR1C3 (also known as Prostaglandin F synthase) that probably enhances the fitness of the senescent cells [21]; the level of ER stress that has to be resolved [41]; and the levels of oxidative stress and autophagy -which are strictly linked- which have to be not too high (unless lethal) but much higher than those of exponentially growing cells [19]. Here, we show that invalidation of PTGS2, its pharmacological inhibition, or the inhibition of the EP4 receptor decreased the frequency of neoplastic escape, strongly suggesting that the PTGS2/PGE<sub>2</sub>/EP4 axis is another parameter associated with the early steps of epithelial cell transformation. Therefore, the selective inhibition of PTGS2 or EP4 could be a therapeutic avenue to make regress the preneoplastic lesions that often comprise a high percentage of senescent cells [58, 59], or block their malignant evolution that could operate by senescence evasion. In support to this proposal, it should be noted that high PTGS2 expression was found in actinic keratoses, the pre-neoplastic precursor of squamous cell carcinoma [60, 61]. Interestingly, diclofenac (an inhibitor of PGE<sub>2</sub> synthesis among its mechanism of action) is currently used for the topical treatment of actinic keratoses, with good tolerance and very good efficacy [62–65]. In addition, it was reported that the homozygous deficiency of either PTGS1 or PTGS2 reduces skin tumorigenesis by 75% in a multistage mouse skin model [39].

More generally, there are evidence of a role of the PTGS2/PGE<sub>2</sub> axis in causing and promoting the development of a variety of cancers, including non-melanoma skin cancers (basal cell carcinoma and squamous cell carcinoma) and melanoma [66–69]. Other evidences suggest that EP1, -2, and -4, but not -3, play a role in tumorigenesis [48]. Our results indicate that EP4 would be the principal EP receptor by which PGE<sub>2</sub> exerts its effects on NHEK senescence. This is of importance because EP4 has been shown to be a tumor promoting receptor in skin, and in particular, can increase melanoma proliferation and metastasis [70]. In contrast, the inhibition of the EP4 receptor has been shown to inhibit tumor growth, angiogenesis, lymph angiogenesis, and metastasis [71].

In conclusion, we report that in epidermal keratinocytes, the PTGS2/PGE<sub>2</sub>/EP4 pathway plays a regulatory role in senescence, and regulates the mechanism of pre-transformation by senescence evasion, depending on its level of activation. Moreover, our findings confirm that prostaglandins are components of the SASP [35, 38, 72], possibly contributing to its inflammatory and protumorigenic effect together with cytokines, growth factors and MMPs already described. These results may provide a

foundation for future anti-aging and anti-cancer therapeutic approaches. Since carcinomas often develop in the context of advanced age, a specific pharmacological inhibition of the PGE<sub>2</sub> pathway might represent a useful strategy to, at the same time, eliminate the senescent pre-cancerous cells of pre-neoplastic lesions such as actinic keratosis, prevent their switch from senescence to pre-transformation, and reduce the global inflammatory context of aging that favors the growth of cancer cells.

## MATERIALS AND METHODS

### Reagents and cell culture

Normal human epidermal keratinocytes (NHEKs) were purchased from Lonza (Basel, Switzerland), Clonetics (CC-2501), or Promocell (Heidelberg, Germany). We used cells from 6 different donors from various ethnic origin and age (referred as 4F0315, K3MC1, K23FC1, K40FH1, K67FA1, KNBMC1). Cells were obtained anonymously and informed consent of each skin donor was obtained by the supplier. Cells were grown at 37°C in an atmosphere of 5% CO<sub>2</sub> in a KGM-2 BulletKit medium consisting of modified MCB153 with 0,15 mmol/L calcium, supplemented with bovine pituitary extract, epidermal growth factor, insulin, hydrocortisone, transferrin, and epinephrin (Clonetics). Such a serum-free low-calcium medium was shown to minimize keratinocyte terminal differentiation [73]. In all experiments, cells were seeded at 3500 cells/cm<sup>2</sup> and always splitted at 70% confluence. The number of population doublings (PDs) was calculated at each passage by means of the following equation:  $PD = \log(\text{number of collected cells}/\text{number of plated cells})/\log 2$ . The exponential growth phase is defined as the phase during which cells divide regularly, do not display the enlarged and spread morphology nor express the SA- $\beta$ -Gal marker. Depending on the donor, the senescent stage was reached after a slightly different number of population doublings. NHEKs were considered senescent when having reached a growth plateau during which they display increased cell size, polynucleation, accumulation of vacuoles and various damaged components, and SA- $\beta$ -Gal activity, as described in [18]. Emergent cells resulted from an atypical budding mitosis generating clones of PSNE cells as described in [22].

NS398, rofecoxib, PGE<sub>2</sub>, were obtained from Sigma (St Louis, MO), EP1 antagonist (AH6809, dissolved in DMSO), EP4 antagonist (L-161,982, dissolved in DMSO), EP1 agonist (iloprost, dissolved in DMSO), EP4 agonists (L-902,688, dissolved in ethanol; Rivenprost, dissolved in methyl acetate) were purchased from Cayman Chemicals (Ann Arbor, MI, USA).

### Prostanoid competitive assays

Young and senescent NHEKs transfected by siRNAs or exposed to the indicated drugs were seeded at 20,000 cells per well in 6-well plates. The culture medium was changed every day. PGE<sub>2</sub>, PGD<sub>2</sub> and PGF<sub>2</sub> $\alpha$  levels in the supernatant medium were assayed at day 4 after transfection by using respectively a prostaglandin E2 Kit (RPN222, Amersham Cytiva), prostaglandin D2 kit (E4718-100 BioVision), prostaglandin F<sub>2</sub> $\alpha$  kit (Abcam, ab133056), according to manufacturer's instructions. The concentration of PGE<sub>2</sub>, PGD<sub>2</sub> and PGF<sub>2</sub> $\alpha$  measured in the culture medium corresponds to the PGE<sub>2</sub>, PGD<sub>2</sub> and PGF<sub>2</sub> $\alpha$  secreted and accumulated in the culture medium during 24 h. Once seeded, the NHEKs are recounted when collecting the conditioned media. Then, the conditioned medium of the exponentially growing NHEKs is diluted with complete culture medium, in order to have equivalent numbers of cells between the different conditions. Finally, a given volume is used for the competitive assays. The values obtained are expressed in pg/mL and therefore come from the same number of secreting NHEKs whatever the conditions.

### Immunofluorescence on cells and tissue sections

NHEKs were fixed with 4% paraformaldehyde (PFA) in PBS and permeabilized with 0.2% Triton-X-100. Slides were incubated with the primary antibody diluted in the presence of 5% BSA. They were then washed three times with PBS and incubated with the secondary antibody diluted in PBS with 0.5% casein. After three washes, nuclei were stained with Hoechst 33258 at 1  $\mu$ g/mL for 3 min. Primary antibodies used were: mouse anti-PTGS2 (Santa Cruz sc-7951, 1:250) and anti-XRCC1 (Abcam, ab1838, 1:500). Secondary antibodies were IgG conjugated with rhodamine or FITC, purchased from Jackson laboratories. Human skin samples were obtained from the SkinAge Project (NCT02553954) at Oscar Lambret Centre (Lille, France), anatomopathology department, according to the French regulations. Skin punch biopsies of 5 mm were obtained from healthy young (18–40 years) and older (55 years and more) subjects (see Supplementary Table 1). The study was approved by local (CPP Nord Ouest) and national (ANSM) ethics committee and subjects gave informed written consent prior to inclusion in this study. Biopsies were embedded with OCT into a plastic cryomolds before freezing. After frozen sectioning (6  $\mu$ m) on a microtome-cryostat, sections were mounted onto slides for analysis. Sections were fixed in PFA 4% for 10 min, and washed in PBS. Non-specific binding was blocked by incubation in 5% bovine serum albumin in PBS. Primary antibody was incubated for 1 h at 37°C or overnight at 4°C. The used antibodies are: anti-PTGS2 (Santa Cruz, sc-7951, 1:50),

anti-XRCC1 (Abcam, ab1838, 1:200), anti-EP1 (Cayman Chemical, 101740, 1:500), and anti-EP4 (Cayman Chemical, 101775, 1:400). After washings in PBS, tissue sections were incubated with AlexaFluor 488 anti-IgG Rabbit (A21206; Molecular Probes) or AlexaFluor 488 anti-IgG Mouse (A-21202, Molecular Probes) for 60 min at RT. Finally, tissue sections were washed in PBS, nuclei were stained for 5 min with DAPI (Roche, Life Science Products, Basel, Switzerland) at 1 µg/mL and mounted in Glycergel (Dako). Optical sectioning images were taken using LSM 780 Confocal Microscope (Zeiss, Germany). AxioVision or ZEN software (Zeiss) were used for microscope image analysis.

### Epidermis fluorescence quantification

The mean PTGS2 fluorescence of each skin layer was measured using ImageJ. The boundaries of each cell in the basal layer (BL) were delimited using the drawing/selection tools of ImageJ. The « area integrated density » and the « mean grey value » were established for each cell. Then, the corrected total cell fluorescence (CTCF) was calculated using the formula  $CTCF = \text{Integrated Density} - (\text{Area of selected cell} \times \text{Mean fluorescence of background})$ . The mean fluorescence of the background was obtained by selecting multiple regions with no fluorescence then calculating the average level of the grey value. A minimum of 25 cells per layer were selected individually in order to obtain a mean fluorescence per layer.

### Cytokine array and ELISA

To prepare NHEKs-conditioned medium (NHEK-CM), we plated a total of  $2 \times 10^6$  cells onto 100 mm plates. Twenty-four hours later, the complete culture medium

was replaced with 10 mL basal KGM2 medium. After another 24 hours, the supernatant was aspirated gently, filtered through a 0.22 µm filter, transferred to ultrafiltration conical tubes (Amicon Ultra-15 with membranes selective for 3 kDa), and centrifuged to concentrate the NHEK-CM. Control medium (KGM2) was generated in the same way except there were no cells in the plate. Cytokine array assay (Proteome Profiler Human Cytokine Array, R&D systems, ARY005B, Minneapolis, MN, USA) was performed as described by the manufacturer. IL-10 (D1000B, R&D Systems, Minneapolis, MN, USA), GM-CSF (Abcam, ab174448) and G-CSF (Abcam, ab188390) ELISA assays were performed according to the manufacturer's instructions. Once seeded, the NHEKs are recounted when collecting the conditioned media. Then, the conditioned medium of the exponentially growing NHEKs is diluted with complete culture medium, in order to have equivalent numbers of cells between the different conditions. Finally, a given volume is used for the ELISA assays. The values obtained are expressed in pg/mL and therefore come from the same number of secreting NHEKs whatever the conditions.

### RNA isolation, reverse transcription, PCR and quantitative real-time PCRs (qRT-PCR)

Total RNAs were extracted using RNeasy mini-columns (QIAGEN, Venlo, Netherlands). One µg of RNA was reverse-transcribed using random hexamers, Superscript III and dNTPs (Life Technologies, Carlsbad, NM, USA) in a final volume of 20 µl according to manufacturer's instructions. Quantitative real-time PCR reactions were performed using the Mx3005P Real-time PCR system (Stratagen, Kirkland, WA, USA). Primer's sequences are listed below.

Name	FWD	REV
PTGES1	5'-GAGTAGACGAAGCCCAGGAA-3'	5'-AGTATTGCAGGAGCGACCC-3'
PTGES2	5'-CTGCAGAAGGGACACGTCTT-3'	5'-AGGACCTCCACGCAGAGC-3'
PTGS2	5'-CAAATCCTTGCTGTTCCACCCAT-3'	5'-GTGCACTGTGTTTGGAGTGGGTTT-3'
PTGDS	5'-CCTACTCCGTGTCAGTGGTG-3'	5'-TCCGTCATGCACTTATCGGTT-3'
PGFS	5'-GAGACAAACGATGGGTGGACC-3'	5'-TGGAAC TCAAAAACCTGCACG-3'
PGIS	5'-CACACCTGTGCTTGATAGCG-3'	5'-GTCGCAGGTTGAATTCTCGC-3'
TXAS1	5'-GTGATGTTTGTCTGGTTGCCT-3'	5'-CCAAGAGAGCCACTGACAGG-3'
EAR	5'-GAGGCTGAGGCAGGAGAATCG-3'	5'-GTCGCCAGGCTGGAGTG-3'

PCR products were measured by SYBR Green fluorescence (SYBR Green Master Mix, Applied Biosystems, Waltham, MA, USA). Experiments were performed in triplicates for each data point. Results were analyzed with the MxPro software (Agilent, Santa Clara, CA, USA). Expressed Alu Repeats (EAR) was used as an endogenous control to normalize the target gene expression, and fold expression relative to the

control is shown. Semi-quantitative RT-PCR were performed with primers for EP1, EP3 and EP4 that were synthesized following (Han et al., 2005). Primers for EP2 were designed using DNASTAR (Genbank N° U19487) and were as follow: EP2 forward 5'-GCGCA TCTCTTTTCCAGGCACCCACCAT-3', EP2 reverse 5'-CATAGTCCAGCAGCGGCAGCGAGCAG AAGA-3'.

## Western-blotting

Equal numbers of young, senescent or emergent NHEKs were lysed in Laemmli buffer 2X containing SDS 4%, Glycerol 20%, Tris-HCl 50 mM pH 6.8, bromophenol blue 0.02% and 2-Mercaptoethanol 5%. Samples were denatured by heating at 95°C for 5 min. Proteins were resolved by SDS-PAGE and transferred to nitrocellulose membranes (Hybond-C extra, Amersham). Primary antibodies used were anti-human PTGS2 (Santa Cruz Biotechnology), anti-human MnSOD (Calbiochem, Darmstadt, Germany, 574596), anti-human PCNA (Dako Cytomatio, Glostrup, Denmark, M0879), anti-human GPX4 (Santa Cruz Biotechnology), anti-human PTGES1 (Santa-Cruz Biotechnology), anti-human p16<sup>INK4</sup> (BD Pharmingen), and anti-human GAPDH (Chemicon International, Billerica, MA, USA). Secondary antibodies used were peroxidase-conjugated (Jackson Immuno-Research Laboratories, West Grove, PA, USA). Peroxidase activity was revealed using ECL (enhanced chemiluminescence) or ECL advanced kits (Amersham Biosciences, Piscataway, NJ, USA).

## Small interference RNA

Invalidation experiments for PTGS2, PTGSE1, PTGDS, PGFS were performed using pools of siRNAs from Dharmacon (ON TARGET Plus Smart pool, Dharmacon, Lafayette, CO, USA). A non-targeting siRNA pool (Dharmacon) was used as control. Proliferating, senescent were plated at 70,000 cells per well in six-well plates and were transfected by using the RNAiMAX Lipofectamine reagent (Invitrogen Corp., Carlsbad, CA, USA) or by using PrimeFect siRNA Transfection Reagent (Lonza) according to manufacturer's instructions.

## Measurement of SA-β-Gal activity

The SA-β-Gal activity was revealed as described by [37]. Briefly, Cells were fixed with 2% formaldehyde/0.2% glutaraldehyde in PBS for 10 min at room temperature. After a rapid wash with PBS, cells were incubated at 37°C overnight in the X-Gal reaction mixture (1 mg/mL X-Gal, 40 mM phosphate buffer (pH 6), 5 mM potassium ferrocyanide, 5 mM potassium ferricyanide, 150 mM NaCl, 2 mM MgCl<sub>2</sub>). The blue cells considered as SA-β-Gal positive were manually counted in at least five independent fields for a total of at least 100 cells for each condition.

## Measure of ROS levels

The oxidant status NHEKs was assessed using H<sub>2</sub>DCFDA (2',7'-dichlorofluorescein diacetate) (D399, Molecular Probes), which diffuses across membranes and is oxidized to fluorescent DCF. Exponentially

growing and senescent NHEKs were incubated with 5 μM H<sub>2</sub>DCFDA diluted in KGM-2 medium for 15 min at 37°C. Fluorescence was read either on adherent cells using a fluorimeter (Fluostar Optima from BMG Labtech, Ortenberg, Germany), or using a flow cytometer (Coulter EPICS XL-MCL) after trypsinization, washing, and resuspension in prewarmed PBS at 37°C.

## Calculation of PSNE frequency

After chemical treatment, senescent NHEKs were seeded into 10 cm dishes at the limit density for emergence (2,000 cells per dish). A few days later, the dishes were fixed and stained by crystal violet, the emergent clones were counted under microscopic examination, as described in [22].

## Statistical analyses

Student's one- or two-tailed *t*-tests, as appropriate, were used for statistical analyses. The *p*-values are indicated in the diagrams with \* for *p*-values < 0.05, \*\* for *p*-values < 0.01 or \*\*\* for *p*-values < 0.001.

## Abbreviations

PTGS2: prostaglandin-endoperoxide synthase 2; PG: prostaglandin; PSNE: post-senescence neoplastic escape; EP 1 to 4: prostaglandin receptor 1 to 4; SA-β-Gal: senescence-associated β-galactosidase; NHEK: normal human epidermal keratinocyte; SASP: senescence-associated secretory phenotype; PGE<sub>2</sub>: prostaglandin E<sub>2</sub>; PGH<sub>2</sub>: prostaglandin H<sub>2</sub>; PGD<sub>2</sub>: prostaglandin D<sub>2</sub>; PGF<sub>2α</sub>: prostaglandin F<sub>2α</sub>; NSAIDs: non-steroidal anti-inflammatory drugs; TX: thromboxane; MnSOD: manganese superoxide dismutase; GPX4: glutathione-peroxidase 4; ROS: reactive oxygen species; H<sub>2</sub>DCFDA: Dichlorodihydrofluorescein-diacetate; CM: conditioned medium; NHDF: Normal human dermal fibroblast; SCC: squamous cell carcinoma; AK: actinic keratoses; MMP: matrix metalloprotease.

## AUTHOR CONTRIBUTIONS

ES and OP designed the study. ES, NM, CD, CDS, JG, AP, JD, LS, JN, CV, and CSC performed the experiments. GD, NP, and JT provided the samples from patients. ES, NM, CD, CA, and OP analyzed the data. CA and OP interpreted the data and wrote the manuscript. All authors read and approved the final version of the manuscript.

## ACKNOWLEDGMENTS

The authors thank Dr. Florence Debacq-Chainiaux critical reading of the manuscript.

## CONFLICTS OF INTEREST

The authors declare no conflicts of interest related to this study.

## ETHICAL STATEMENT AND CONSENT

The study was approved by local (CPP Nord Ouest) and National (ANSM) Ethics Committee and subjects gave informed written consent prior to inclusion in this study (Approval Number: NCT02553954).

## FUNDING

This work was supported by grants from the Association pour la Recherche sur le Cancer (ARC), the Ligue contre le Cancer (Comité du Nord et Comité de la Somme), the Contrat de Plan État Région—CTRL (Centre Transdisciplinaire de Recherche sur la Longévité), the Contrat de Plan Etat Région Cancer 2015–2020, an International Research Project (IRP) grant from Inserm, and a Hubert Curien Partnership (PHC) grant implemented by the French Ministry of Europe and Foreign Affairs, and the French Ministry of Higher Education and Research to Olivier Pluquet. JN was recipient of a doctoral fellowship from the University of Lille and from the ARC foundation. AP is recipient of a doctoral fellowship from the Région Hauts-de-France and the University of Lille. Joëlle Giroud was supported by a co-funded FSR fellowship (UNamur) and doctoral fellowship (Univ Lille). The Canther laboratory is part of the OncoLille Institute, of the Institut National de la Santé et de la Recherche Médicale (Inserm), of the Centre National de la Recherche Scientifique (CNRS), of the Université de Lille, and of the Institut Pasteur de Lille.

## REFERENCES

1. Lewis DA, Travers JB, Machado C, Somani AK, Spandau DF. Reversing the aging stromal phenotype prevents carcinoma initiation. *Aging* (Albany NY). 2011; 3:407–16.  
<https://doi.org/10.18632/aging.100318>  
PMID:21515933
2. Herbig U, Ferreira M, Condell L, Carey D, Sedivy JM. Cellular senescence in aging primates. *Science*. 2006; 311:1257.  
<https://doi.org/10.1126/science.1122446>  
PMID:16456035
3. Maru GB, Gandhi K, Ramchandani A, Kumar G. The role of inflammation in skin cancer. *Adv Exp Med Biol*. 2014; 816:437–69.  
[https://doi.org/10.1007/978-3-0348-0837-8\\_17](https://doi.org/10.1007/978-3-0348-0837-8_17)  
PMID:24818733

4. Jayapalan JC, Ferreira M, Sedivy JM, Herbig U. Accumulation of senescent cells in mitotic tissue of aging primates. *Mech Ageing Dev*. 2007; 128:36–44.  
<https://doi.org/10.1016/j.mad.2006.11.008>  
PMID:17116315
5. Kaldor J, Shugg D, Young B, Dwyer T, Wang YG. Non-melanoma skin cancer: ten years of cancer-registry-based surveillance. *Int J Cancer*. 1993; 53:886–91.  
<https://doi.org/10.1002/ijc.2910530603>  
PMID:8473047
6. Pluquet O, Poutier A, Abbadie C. The unfolded protein response and cellular senescence. A review in the theme: cellular mechanisms of endoplasmic reticulum stress signaling in health and disease. *Am J Physiol Cell Physiol*. 2015; 308:C415–25.  
<https://doi.org/10.1152/ajpcell.00334.2014>  
PMID:25540175
7. Hernandez-Segura A, Nehme J, Demaria M. Hallmarks of Cellular Senescence. *Trends Cell Biol*. 2018; 28:436–53.  
<https://doi.org/10.1016/j.tcb.2018.02.001>  
PMID:29477613
8. Kumari R, Jat P. Mechanisms of Cellular Senescence: Cell Cycle Arrest and Senescence Associated Secretory Phenotype. *Front Cell Dev Biol*. 2021; 9:645593.  
<https://doi.org/10.3389/fcell.2021.645593>  
PMID:33855023
9. Stein GH, Drullinger LF, Souillard A, Dulić V. Differential roles for cyclin-dependent kinase inhibitors p21 and p16 in the mechanisms of senescence and differentiation in human fibroblasts. *Mol Cell Biol*. 1999; 19:2109–17.  
<https://doi.org/10.1128/MCB.19.3.2109>  
PMID:10022898
10. Alcorta DA, Xiong Y, Phelps D, Hannon G, Beach D, Barrett JC. Involvement of the cyclin-dependent kinase inhibitor p16 (INK4a) in replicative senescence of normal human fibroblasts. *Proc Natl Acad Sci U S A*. 1996; 93:13742–7.  
<https://doi.org/10.1073/pnas.93.24.13742>  
PMID:8943005
11. Roger L, Tomas F, Gire V. Mechanisms and Regulation of Cellular Senescence. *Int J Mol Sci*. 2021; 22:13173.  
<https://doi.org/10.3390/ijms222313173>  
PMID:34884978
12. Abbadie C, Pluquet O, Poutier A. Epithelial cell senescence: an adaptive response to pre-carcinogenic stresses? *Cell Mol Life Sci*. 2017; 74:4471–509.  
<https://doi.org/10.1007/s00018-017-2587-9>  
PMID:28707011
13. Ben-Porath I, Weinberg RA. The signals and pathways activating cellular senescence. *Int J Biochem Cell Biol*. 2005; 37:961–76.

- <https://doi.org/10.1016/j.biocel.2004.10.013>  
PMID:15743671
14. Kuilman T, Michaloglou C, Mooi WJ, Peeper DS. The essence of senescence. *Genes Dev.* 2010; 24:2463–79.  
<https://doi.org/10.1101/gad.1971610>  
PMID:21078816
15. Coppé JP, Patil CK, Rodier F, Sun Y, Muñoz DP, Goldstein J, Nelson PS, Desprez PY, Campisi J. Senescence-associated secretory phenotypes reveal cell-nonautonomous functions of oncogenic RAS and the p53 tumor suppressor. *PLoS Biol.* 2008; 6:2853–68.  
<https://doi.org/10.1371/journal.pbio.0060301>  
PMID:19053174
16. Giroud J, Bouriez I, Paulus H, Pourtier A, Debacq-Chainiaux F, Pluquet O. Exploring the Communication of the SASP: Dynamic, Interactive, and Adaptive Effects on the Microenvironment. *Int J Mol Sci.* 2023; 24:10788.  
<https://doi.org/10.3390/ijms241310788>  
PMID:37445973
17. Yang J, Liu M, Hong D, Zeng M, Zhang X. The Paradoxical Role of Cellular Senescence in Cancer. *Front Cell Dev Biol.* 2021; 9:722205.  
<https://doi.org/10.3389/fcell.2021.722205>  
PMID:34458273
18. Gosselin K, Deruy E, Martien S, Vercamer C, Bouali F, Dujardin T, Slomianny C, Houel-Renault L, Chelli F, De Launoit Y, Abbadie C. Senescent keratinocytes die by autophagic programmed cell death. *Am J Pathol.* 2009; 174:423–35.  
<https://doi.org/10.2353/ajpath.2009.080332>  
PMID:19147823
19. Deruy E, Nassour J, Martin N, Vercamer C, Malaquin N, Bertout J, Chelli F, Pourtier A, Pluquet O, Abbadie C. Level of macroautophagy drives senescent keratinocytes into cell death or neoplastic evasion. *Cell Death Dis.* 2014; 5:e1577.  
<https://doi.org/10.1038/cddis.2014.533>  
PMID:25522271
20. Deruy E, Gosselin K, Vercamer C, Martien S, Bouali F, Slomianny C, Bertout J, Bernard D, Pourtier A, Abbadie C. MnSOD upregulation induces autophagic programmed cell death in senescent keratinocytes. *PLoS One.* 2010; 5:e12712.  
<https://doi.org/10.1371/journal.pone.0012712>  
PMID:20856861
21. Martin N, Salazar-Cardozo C, Vercamer C, Ott L, Marot G, Slijepcevic P, Abbadie C, Pluquet O. Identification of a gene signature of a pre-transformation process by senescence evasion in normal human epidermal keratinocytes. *Mol Cancer.* 2014; 13:151.  
<https://doi.org/10.1186/1476-4598-13-151>  
PMID:24929818
22. Gosselin K, Martien S, Pourtier A, Vercamer C, Ostoich P, Morat L, Sabatier L, Duprez L, T'kint de Roodenbeke C, Gilson E, Malaquin N, Wernert N, Slijepcevic P, et al. Senescence-associated oxidative DNA damage promotes the generation of neoplastic cells. *Cancer Res.* 2009; 69:7917–25.  
<https://doi.org/10.1158/0008-5472.CAN-08-2510>  
PMID:19826058
23. Malaquin N, Vercamer C, Bouali F, Martien S, Deruy E, Wernert N, Chwastyniak M, Pinet F, Abbadie C, Pourtier A. Senescent fibroblasts enhance early skin carcinogenic events via a paracrine MMP-PAR-1 axis. *PLoS One.* 2013; 8:e63607.  
<https://doi.org/10.1371/journal.pone.0063607>  
PMID:23675494
24. Smith WL, DeWitt DL, Garavito RM. Cyclooxygenases: structural, cellular, and molecular biology. *Annu Rev Biochem.* 2000; 69:145–82.  
<https://doi.org/10.1146/annurev.biochem.69.1.145>  
PMID:10966456
25. Narumiya S, Sugimoto Y, Ushikubi F. Prostanoid receptors: structures, properties, and functions. *Physiol Rev.* 1999; 79:1193–226.  
<https://doi.org/10.1152/physrev.1999.79.4.1193>  
PMID:10508233
26. Simmons DL, Botting RM, Hla T. Cyclooxygenase isozymes: the biology of prostaglandin synthesis and inhibition. *Pharmacol Rev.* 2004; 56:387–437.  
<https://doi.org/10.1124/pr.56.3.3>  
PMID:15317910
27. Loftin CD, Tian HF, Langenbach R. Phenotypes of the COX-deficient mice indicate physiological and pathophysiological roles for COX-1 and COX-2. *Prostaglandins Other Lipid Mediat.* 2002; 68-69:177–85.  
[https://doi.org/10.1016/s0090-6980\(02\)00028-x](https://doi.org/10.1016/s0090-6980(02)00028-x)  
PMID:12432917
28. Mitchell JA, Evans TW. Cyclooxygenase-2 as a therapeutic target. *Inflamm Res.* 1998 (Suppl 2); 47:S88–92.  
<https://doi.org/10.1007/s000110050287>  
PMID:9831329
29. Funk CD, FitzGerald GA. COX-2 inhibitors and cardiovascular risk. *J Cardiovasc Pharmacol.* 2007; 50:470–9.  
<https://doi.org/10.1097/FJC.0b013e318157f72d>  
PMID:18030055
30. Cha YI, DuBois RN. NSAIDs and cancer prevention: targets downstream of COX-2. *Annu Rev Med.* 2007; 58:239–52.

<https://doi.org/10.1146/annurev.med.57.121304.131253>

PMID:[17100552](https://pubmed.ncbi.nlm.nih.gov/17100552/)

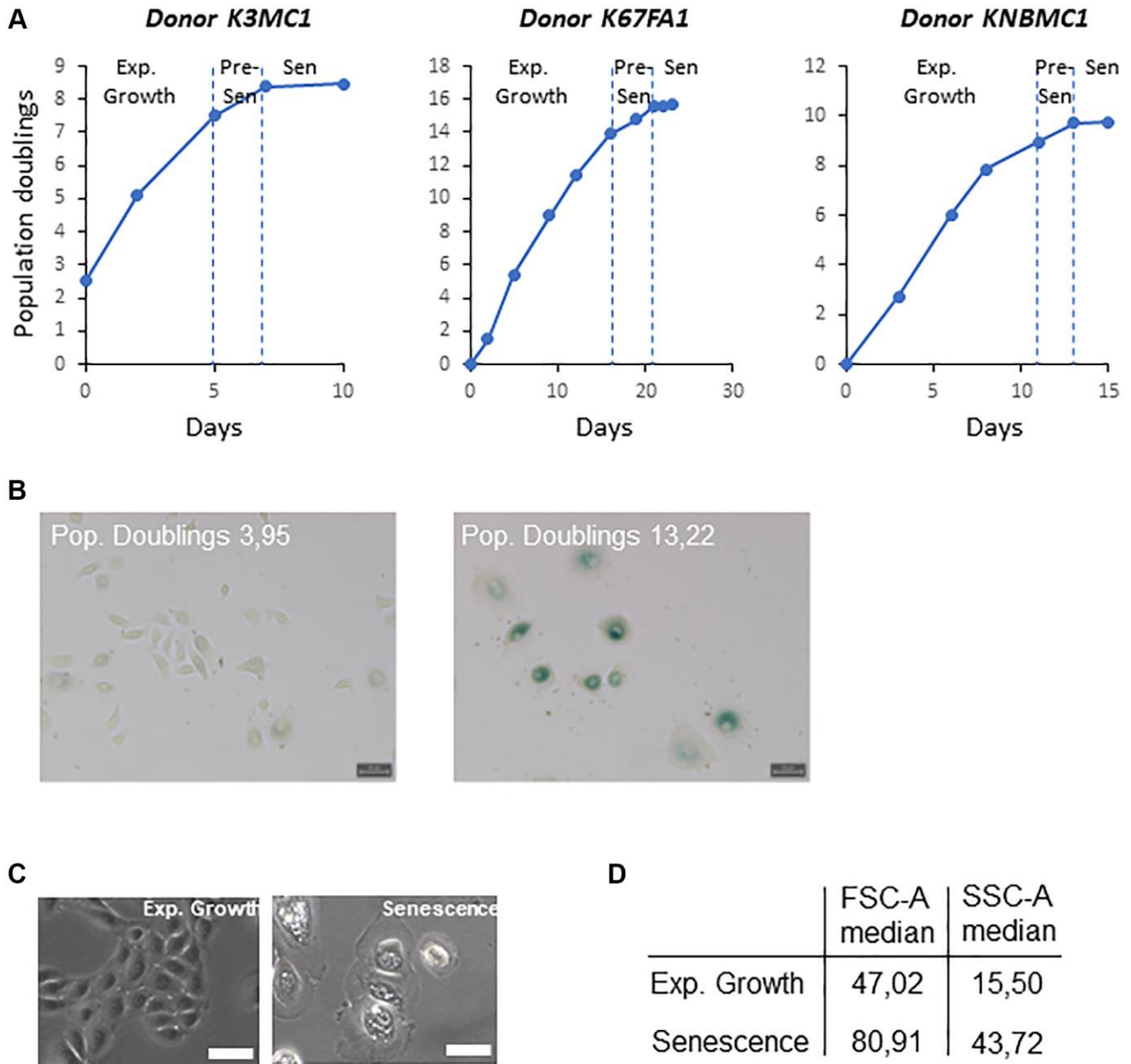
31. Wang D, Dubois RN. Eicosanoids and cancer. *Nat Rev Cancer*. 2010; 10:181–93.  
<https://doi.org/10.1038/nrc2809>  
PMID:[20168319](https://pubmed.ncbi.nlm.nih.gov/20168319/)
32. Habib MA, Salem SA, Hakim SA, Shalan YA. Comparative immunohistochemical assessment of cutaneous cyclooxygenase-2 enzyme expression in chronological aging and photoaging. *Photodermatol Photoimmunol Photomed*. 2014; 30:43–51.  
<https://doi.org/10.1111/phpp.12087>  
PMID:[24393208](https://pubmed.ncbi.nlm.nih.gov/24393208/)
33. Li Y, Lei D, Swindell WR, Xia W, Weng S, Fu J, Worthen CA, Okubo T, Johnston A, Gudjonsson JE, Voorhees JJ, Fisher GJ. Age-Associated Increase in Skin Fibroblast-Derived Prostaglandin E2 Contributes to Reduced Collagen Levels in Elderly Human Skin. *J Invest Dermatol*. 2015; 135:2181–8.  
<https://doi.org/10.1038/jid.2015.157>  
PMID:[25905589](https://pubmed.ncbi.nlm.nih.gov/25905589/)
34. Lee ME, Kim SR, Lee S, Jung YJ, Choi SS, Kim WJ, Han JA. Cyclooxygenase-2 inhibitors modulate skin aging in a catalytic activity-independent manner. *Exp Mol Med*. 2012; 44:536–44.  
<https://doi.org/10.3858/emm.2012.44.9.061>  
PMID:[22771771](https://pubmed.ncbi.nlm.nih.gov/22771771/)
35. Zdanov S, Bernard D, Debacq-Chainiaux F, Martien S, Gosselin K, Vercamer C, Chelli F, Toussaint O, Abbadie C. Normal or stress-induced fibroblast senescence involves COX-2 activity. *Exp Cell Res*. 2007; 313:3046–56.  
<https://doi.org/10.1016/j.yexcr.2007.04.033>  
PMID:[17560572](https://pubmed.ncbi.nlm.nih.gov/17560572/)
36. Kim SR, Park JH, Lee ME, Park JS, Park SC, Han JA. Selective COX-2 inhibitors modulate cellular senescence in human dermal fibroblasts in a catalytic activity-independent manner. *Mech Ageing Dev*. 2008; 129:706–13.  
<https://doi.org/10.1016/j.mad.2008.09.003>  
PMID:[18848576](https://pubmed.ncbi.nlm.nih.gov/18848576/)
37. Martien S, Pluquet O, Vercamer C, Malaquin N, Martin N, Gosselin K, Pourtier A, Abbadie C. Cellular senescence involves an intracrine prostaglandin E2 pathway in human fibroblasts. *Biochim Biophys Acta*. 2013; 1831:1217–27.  
<https://doi.org/10.1016/j.bbailip.2013.04.005>  
PMID:[24046862](https://pubmed.ncbi.nlm.nih.gov/24046862/)
38. Gonçalves S, Yin K, Ito Y, Chan A, Olan I, Gough S, Cassidy L, Serrao E, Smith S, Young A, Narita M, Hoare M. COX2 regulates senescence secretome composition and senescence surveillance through PGE<sub>2</sub>. *Cell Rep*. 2021; 34:108860.  
<https://doi.org/10.1016/j.celrep.2021.108860>  
PMID:[33730589](https://pubmed.ncbi.nlm.nih.gov/33730589/)
39. Tiano HF, Loftin CD, Akunda J, Lee CA, Spalding J, Sessoms A, Dunson DB, Rogan EG, Morham SG, Smart RC, Langenbach R. Deficiency of either cyclooxygenase (COX)-1 or COX-2 alters epidermal differentiation and reduces mouse skin tumorigenesis. *Cancer Res*. 2002; 62:3395–401.  
PMID:[12067981](https://pubmed.ncbi.nlm.nih.gov/12067981/)
40. Nassour J, Martien S, Martin N, Deruy E, Tomellini E, Malaquin N, Bouali F, Sabatier L, Wernert N, Pinte S, Gilson E, Pourtier A, Pluquet O, Abbadie C. Defective DNA single-strand break repair is responsible for senescence and neoplastic escape of epithelial cells. *Nat Commun*. 2016; 7:10399.  
<https://doi.org/10.1038/ncomms10399>  
PMID:[26822533](https://pubmed.ncbi.nlm.nih.gov/26822533/)
41. Drullion C, Marot G, Martin N, Desle J, Saas L, Salazar-Cardozo C, Bouali F, Pourtier A, Abbadie C, Pluquet O. Pre-malignant transformation by senescence evasion is prevented by the PERK and ATF6alpha branches of the Unfolded Protein Response. *Cancer Lett*. 2018; 438:187–96.  
<https://doi.org/10.1016/j.canlet.2018.09.008>  
PMID:[30213560](https://pubmed.ncbi.nlm.nih.gov/30213560/)
42. Legrain Y, Touat-Hamici Z, Chavatte L. Interplay between selenium levels, selenoprotein expression, and replicative senescence in WI-38 human fibroblasts. *J Biol Chem*. 2014; 289:6299–310.  
<https://doi.org/10.1074/jbc.M113.526863>  
PMID:[24425862](https://pubmed.ncbi.nlm.nih.gov/24425862/)
43. Marnett LJ, Wlodawer P, Samuelsson B. Co-oxygenation of organic substrates by the prostaglandin synthetase of sheep vesicular gland. *J Biol Chem*. 1975; 250:8510–7.  
PMID:[811656](https://pubmed.ncbi.nlm.nih.gov/811656/)
44. Kontos HA, Wei EP, Povlishock JT, Dietrich WD, Magiera CJ, Ellis EF. Cerebral arteriolar damage by arachidonic acid and prostaglandin G<sub>2</sub>. *Science*. 1980; 209:1242–5.  
<https://doi.org/10.1126/science.7403881>  
PMID:[7403881](https://pubmed.ncbi.nlm.nih.gov/7403881/)
45. Egan RW, Paxton J, Kuehl FA Jr. Mechanism for irreversible self-deactivation of prostaglandin synthetase. *J Biol Chem*. 1976; 251:7329–35.  
PMID:[826527](https://pubmed.ncbi.nlm.nih.gov/826527/)
46. Goldyne ME. Cyclooxygenase isoforms in human skin. *Prostaglandins Other Lipid Mediat*. 2000; 63:15–23.  
[https://doi.org/10.1016/s0090-6980\(00\)00094-0](https://doi.org/10.1016/s0090-6980(00)00094-0)  
PMID:[11104338](https://pubmed.ncbi.nlm.nih.gov/11104338/)

47. Machwate M, Harada S, Leu CT, Seedor G, Labelle M, Gallant M, Hutchins S, Lachance N, Sawyer N, Slipetz D, Metters KM, Rodan SB, Young R, Rodan GA. Prostaglandin receptor EP(4) mediates the bone anabolic effects of PGE(2). *Mol Pharmacol*. 2001; 60:36–41.  
<https://doi.org/10.1124/mol.60.1.36>  
PMID:[11408598](https://pubmed.ncbi.nlm.nih.gov/11408598/)
48. Rundhaug JE, Simper MS, Surh I, Fischer SM. The role of the EP receptors for prostaglandin E2 in skin and skin cancer. *Cancer Metastasis Rev*. 2011; 30:465–80.  
<https://doi.org/10.1007/s10555-011-9317-9>  
PMID:[22012553](https://pubmed.ncbi.nlm.nih.gov/22012553/)
49. Campisi J. Cellular senescence as a tumor-suppressor mechanism. *Trends Cell Biol*. 2001; 11:S27–31.  
[https://doi.org/10.1016/s0962-8924\(01\)02151-1](https://doi.org/10.1016/s0962-8924(01)02151-1)  
PMID:[11684439](https://pubmed.ncbi.nlm.nih.gov/11684439/)
50. Baker DJ, Wijshake T, Tchkonja T, LeBrasseur NK, Childs BG, van de Sluis B, Kirkland JL, van Deursen JM. Clearance of p16Ink4a-positive senescent cells delays ageing-associated disorders. *Nature*. 2011; 479:232–6.  
<https://doi.org/10.1038/nature10600>  
PMID:[22048312](https://pubmed.ncbi.nlm.nih.gov/22048312/)
51. Baker DJ, Childs BG, Durik M, Wijers ME, Sieben CJ, Zhong J, Saltness RA, Jeganathan KB, Verzosa GC, Pezeshki A, Khazaie K, Miller JD, van Deursen JM. Naturally occurring p16(Ink4a)-positive cells shorten healthy lifespan. *Nature*. 2016; 530:184–9.  
<https://doi.org/10.1038/nature16932>  
PMID:[26840489](https://pubmed.ncbi.nlm.nih.gov/26840489/)
52. Baar MP, Brandt RMC, Putavet DA, Klein JDD, Derks KWJ, Bourgeois BRM, Stryeck S, Rijksen Y, van Willigenburg H, Feijtel DA, van der Pluijm I, Essers J, van Cappellen WA, et al. Targeted Apoptosis of Senescent Cells Restores Tissue Homeostasis in Response to Chemotoxicity and Aging. *Cell*. 2017; 169:132–47.e16.  
<https://doi.org/10.1016/j.cell.2017.02.031>  
PMID:[28340339](https://pubmed.ncbi.nlm.nih.gov/28340339/)
53. Ching TT, Chiang WC, Chen CS, Hsu AL. Celecoxib extends *C. elegans* lifespan via inhibition of insulin-like signaling but not cyclooxygenase-2 activity. *Aging Cell*. 2011; 10:506–19.  
<https://doi.org/10.1111/j.1474-9726.2011.00688.x>  
PMID:[21348927](https://pubmed.ncbi.nlm.nih.gov/21348927/)
54. Tang EH, Vanhoutte PM. Gene expression changes of prostanoid synthases in endothelial cells and prostanoid receptors in vascular smooth muscle cells caused by aging and hypertension. *Physiol Genomics*. 2008; 32:409–18.  
<https://doi.org/10.1152/physiolgenomics.00136.2007>  
PMID:[18056786](https://pubmed.ncbi.nlm.nih.gov/18056786/)
55. Qian H, Luo N, Chi Y. Aging-shifted prostaglandin profile in endothelium as a factor in cardiovascular disorders. *J Aging Res*. 2012; 2012:121390.  
<https://doi.org/10.1155/2012/121390>  
PMID:[22500225](https://pubmed.ncbi.nlm.nih.gov/22500225/)
56. Kim JW, Zou Y, Yoon S, Lee JH, Kim YK, Yu BP, Chung HY. Vascular aging: molecular modulation of the prostanoid cascade by calorie restriction. *J Gerontol A Biol Sci Med Sci*. 2004; 59:B876–85.  
<https://doi.org/10.1093/gerona/59.9.b876>  
PMID:[15472149](https://pubmed.ncbi.nlm.nih.gov/15472149/)
57. Chen J, Deng JC, Zemans RL, Bahmed K, Kosmider B, Zhang M, Peters-Golden M, Goldstein DR. Age-induced prostaglandin E<sub>2</sub> impairs mitochondrial fitness and increases mortality to influenza infection. *Nat Commun*. 2022; 13:6759.  
<https://doi.org/10.1038/s41467-022-34593-y>  
PMID:[36351902](https://pubmed.ncbi.nlm.nih.gov/36351902/)
58. Yang K, Li X, Xie K. Senescence program and its reprogramming in pancreatic premalignancy. *Cell Death Dis*. 2023; 14:528.  
<https://doi.org/10.1038/s41419-023-06040-3>  
PMID:[37591827](https://pubmed.ncbi.nlm.nih.gov/37591827/)
59. Schmitt CA, Wang B, Demaria M. Senescence and cancer - role and therapeutic opportunities. *Nat Rev Clin Oncol*. 2022; 19:619–36.  
<https://doi.org/10.1038/s41571-022-00668-4>  
PMID:[36045302](https://pubmed.ncbi.nlm.nih.gov/36045302/)
60. Kuźbicki Ł, Lange D, Stanek-Widera A, Chwirot BW. Different expression of cyclooxygenase-2 (COX-2) in selected nonmelanocytic human cutaneous lesions. *Folia Histochem Cytobiol*. 2011; 49:381–8.  
<https://doi.org/10.5603/fhc.2011.0054>  
PMID:[22038215](https://pubmed.ncbi.nlm.nih.gov/22038215/)
61. Nijsten T, Colpaert CG, Vermeulen PB, Harris AL, Van Marck E, Lambert J. Cyclooxygenase-2 expression and angiogenesis in squamous cell carcinoma of the skin and its precursors: a paired immunohistochemical study of 35 cases. *Br J Dermatol*. 2004; 151:837–45.  
<https://doi.org/10.1111/j.1365-2133.2004.06214.x>  
PMID:[15491425](https://pubmed.ncbi.nlm.nih.gov/15491425/)
62. Rivers JK, McLean DI. An open study to assess the efficacy and safety of topical 3% diclofenac in a 2.5% hyaluronic acid gel for the treatment of actinic keratoses. *Arch Dermatol*. 1997; 133:1239–42.  
PMID:[9382562](https://pubmed.ncbi.nlm.nih.gov/9382562/)
63. Rivers JK, Arlette J, Shear N, Guenther L, Carey W, Poulin Y. Topical treatment of actinic keratoses with 3.0% diclofenac in 2.5% hyaluronan gel. *Br J Dermatol*. 2002; 146:94–100.  
<https://doi.org/10.1046/j.1365-2133.2002.04561.x>  
PMID:[11841372](https://pubmed.ncbi.nlm.nih.gov/11841372/)

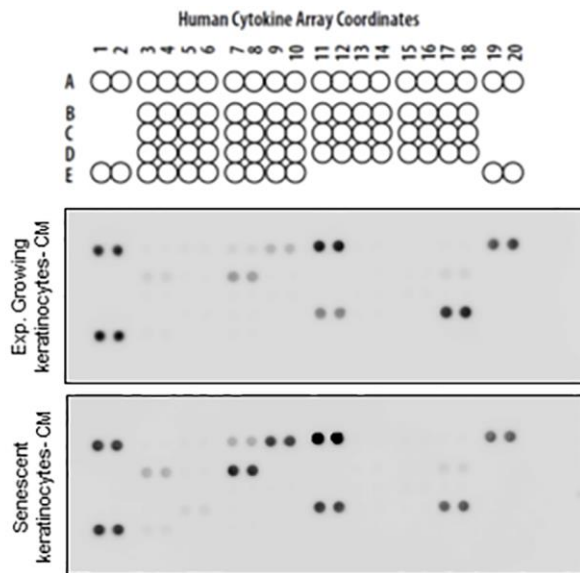
64. Wolf JE Jr, Taylor JR, Tschen E, Kang S. Topical 3.0% diclofenac in 2.5% hyaluronan gel in the treatment of actinic keratoses. *Int J Dermatol*. 2001; 40:709–13. <https://doi.org/10.1046/j.1365-4362.2001.01324.x> PMID:11737438
65. Ulrich M, Pellacani G, Ferrandiz C, Lear JT. Evidence for field cancerisation treatment of actinic keratoses with topical diclofenac in hyaluronic acid. *Eur J Dermatol*. 2014; 24:158–67. <https://doi.org/10.1684/ejd.2014.2286> PMID:24721544
66. An KP, Athar M, Tang X, Katiyar SK, Russo J, Beech J, Aszterbaum M, Kopelovich L, Epstein EH Jr, Mukhtar H, Bickers DR. Cyclooxygenase-2 expression in murine and human nonmelanoma skin cancers: implications for therapeutic approaches. *Photochem Photobiol*. 2002; 76:73–80. [https://doi.org/10.1562/0031-8655\(2002\)076<0073:ceimah>2.0.co;2](https://doi.org/10.1562/0031-8655(2002)076<0073:ceimah>2.0.co;2) PMID:12126310
67. Fischer SM. Is cyclooxygenase-2 important in skin carcinogenesis? *J Environ Pathol Toxicol Oncol*. 2002; 21:183–91. PMID:12086405
68. Elmets CA, Ledet JJ, Athar M. Cyclooxygenases: mediators of UV-induced skin cancer and potential targets for prevention. *J Invest Dermatol*. 2014; 134:2497–502. <https://doi.org/10.1038/jid.2014.192> PMID:24804836
69. Becker MR, Siegelin MD, Rompel R, Enk AH, Gaiser T. COX-2 expression in malignant melanoma: a novel prognostic marker? *Melanoma Res*. 2009; 19:8–16. <https://doi.org/10.1097/CMR.0b013e32831d7f52> PMID:19430402
70. Konya V, Marsche G, Schuligoi R, Heinemann A. E-type prostanoid receptor 4 (EP4) in disease and therapy. *Pharmacol Ther*. 2013; 138:485–502. <https://doi.org/10.1016/j.pharmthera.2013.03.006> PMID:23523686
71. Majumder M, Xin X, Liu L, Girish GV, Lala PK. Prostaglandin E2 receptor EP4 as the common target on cancer cells and macrophages to abolish angiogenesis, lymphangiogenesis, metastasis, and stem-like cell functions. *Cancer Sci*. 2014; 105:1142–51. <https://doi.org/10.1111/cas.12475> PMID:24981602
72. Dagouassat M, Gagliolo JM, Chrusciel S, Bourin MC, Duprez C, Caramelle P, Boyer L, Hue S, Stern JB, Validire P, Longrois D, Norel X, Dubois-Randé JL, et al. The cyclooxygenase-2-prostaglandin E2 pathway maintains senescence of chronic obstructive pulmonary disease fibroblasts. *Am J Respir Crit Care Med*. 2013; 187:703–14. <https://doi.org/10.1164/rccm.201208-1361OC> PMID:23328527
73. Boyce ST, Ham RG. Calcium-regulated differentiation of normal human epidermal keratinocytes in chemically defined clonal culture and serum-free serial culture. *J Invest Dermatol*. 1983; 81:33s–40. <https://doi.org/10.1111/1523-1747.ep12540422> PMID:6345690

SUPPLEMENTARY MATERIALS

Supplementary Figures

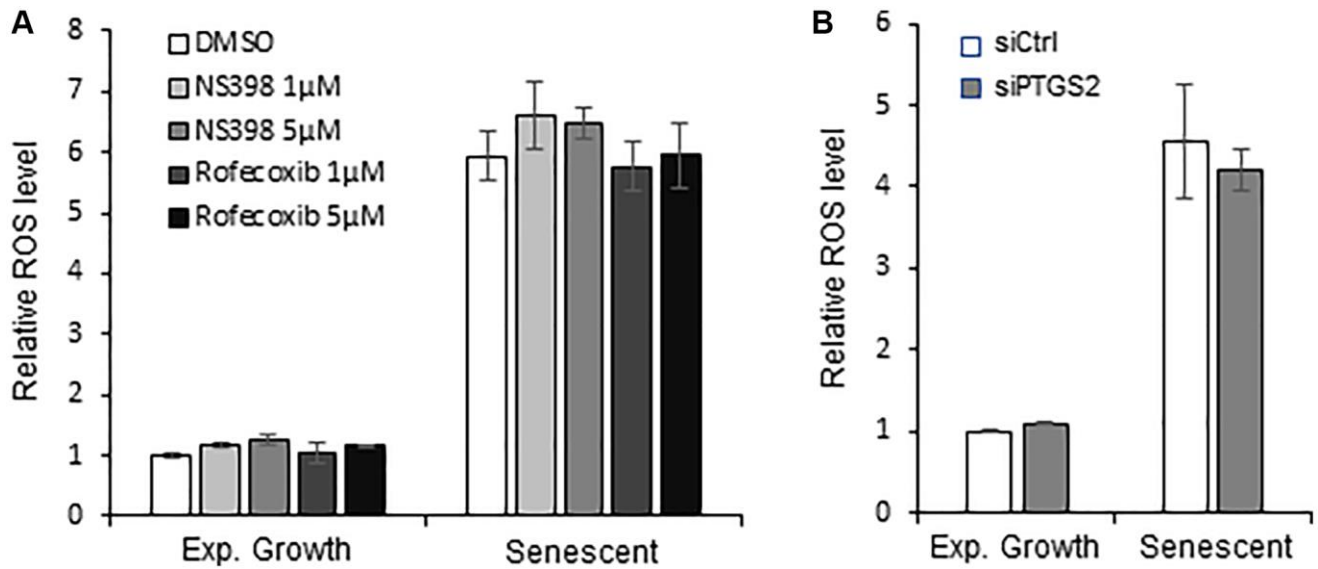


**Supplementary Figure 1. Growth curve and senescence characteristics of *in vitro* cultured NHEKs.** (A) Examples of growth curves of NHEKs (various donors) showing the exponential growth phase, the pre-senescent phase, and the senescence plateau. (B) Representative microscopy images of SA- $\beta$ -Gal staining in exponentially growing and senescent NHEKs (Donor K40FH1). Bar represents 50  $\mu$ m. (C) Cell morphologies observed by phase-contrast microscopy. The images shown illustrate the differences between proliferating and senescent NHEKs, recognizable by their large size and the presence of numerous cytoplasmic refringent or dark vesicles or particles. Bar represents 100  $\mu$ m. (D) Flow cytometric data of NHEKs (K40FH1) at the senescence plateau of forward scatter factor (FSC-A) and side scatter factor (SSC-A).

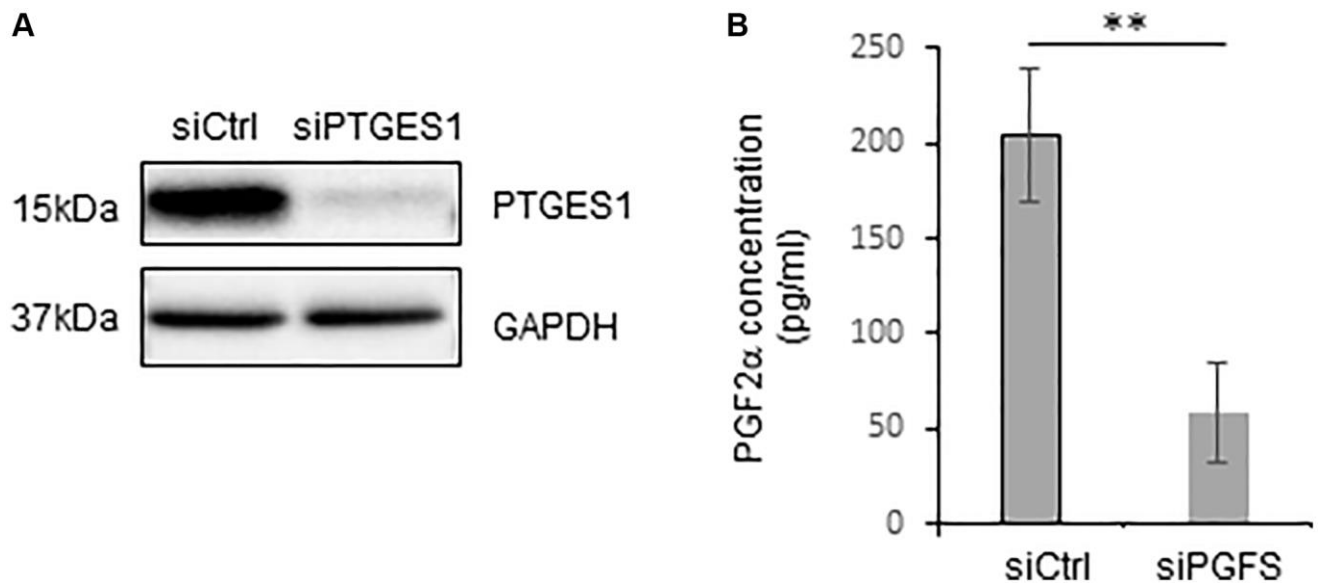


Coordinate	Target/ Control	Exp. Growing NHEKs- CM	Senescent NHEKs-CM	Ratio (Sen/Exp.Growing)		
		Mean Intensity (a.u.)	Mean Intensity (a.u.)			
A3, A4	CCL11/-309	10,7335	10,449	0,9734942		No change
A5, A6	CCL2/MCP-1	12,7225	14,199	1,11605423		Up
A7, A8	MIP-1a/MIP-1b	27,312	34,9235	1,27868702		Down
A9, A10	CCL5/RANTES	35,5275	66,9285	1,88385054		
A11, A12	CD40 Ligand/TNFSF5	96,111	100,356	1,04416768		
A13, A14	Complement Component C5/CSa	10,743	12,534	1,16671321		
A15, A16	CXCL1/GRO $\alpha$	9,6085	12,764	1,32840714		
A17, A18	CXCL10/IP-10	10,1925	11,113	1,0903115		
B3, B4	CXCL11/I-TAC	20,518	32,3985	1,57902817		
B5, B6	CXCL12/SDF-1	11,397	13,457	1,18074932		
B7, B8	G-CSF	58,651	89,4215	1,52463726		
B9, B10	GM-CSF	10,2805	16,3835	1,59364817		
B11, B12	ICAM-1/CD54	9,915	11,4535	1,15516894		
B13, B14	IFN- $\gamma$	9,9505	11,401	1,14577157		
B15, B16	IL-1a/IL-1F1	10,335	12,7075	1,22955975		
B17, B18	IL-1b/IL-1F2	18,4475	21,4725	1,16397886		
C3, C4	IL-1ra/IL-1F3	10,522	12,904	1,22638282		
C5, C6	IL-2	9,79	11,3335	1,15766088		
C7, C8	IL-4	11,0315	12,934	1,17246068		
C9, C10	IL-5	11,5685	13,3665	1,15542205		
C11, C12	IL-6	10,6025	12,431	1,17245933		
C13, C14	IL-8	10,2915	11,92	1,15823738		
C15, C16	IL-10	11,059	13,408	1,21240619		
C17, C18	IL-12 p70	10,93	11,858	1,08490393		
D3, D4	IL-13	9,8245	11,309	1,15110184		
D5, D6	IL-16	10,1265	12,077	1,19261344		
D7, D8	IL-17A	10,8955	12,867	1,18094626		
D9, D10	IL-17E	9,9755	11,387	1,14149667		
D11, D12	IL-18/IL-1F4	75,5645	89,466	1,18396866		
D13, D14	IL-21	10,593	12,0155	1,13428679		
D15, D16	IL-27	10,563	11,1275	1,05344126		
D17, D18	IL-32 $\alpha$	88,964	76,125	0,8556832		
E3, E4	MIF	10,8305	18,343	1,69364295		
E5, E6	Serp in E1/PAI-1	12,88	10,1245	0,78606366		
E7, E8	TN F- $\alpha$	10,3445	11,739	1,13480594		
E9, E10	TR EM-1	9,5195	10,749	1,12915594		

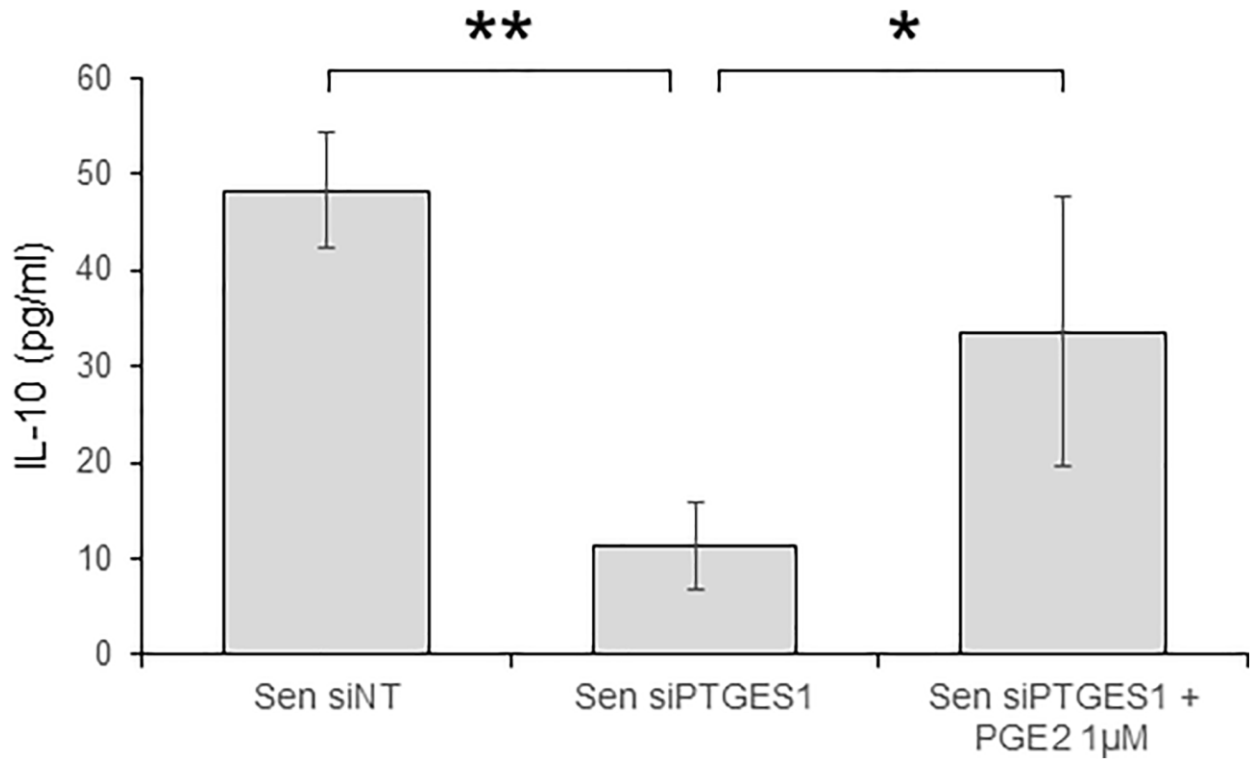
**Supplementary Figure 2. SASP composition in NHEKs.** Cytokine/chemokine array performed with conditioned medium from senescent and exponentially growing NHEKs. The intensity of the signals was quantified by densitometry (ImageJ) and normalized to positive controls for each sample.



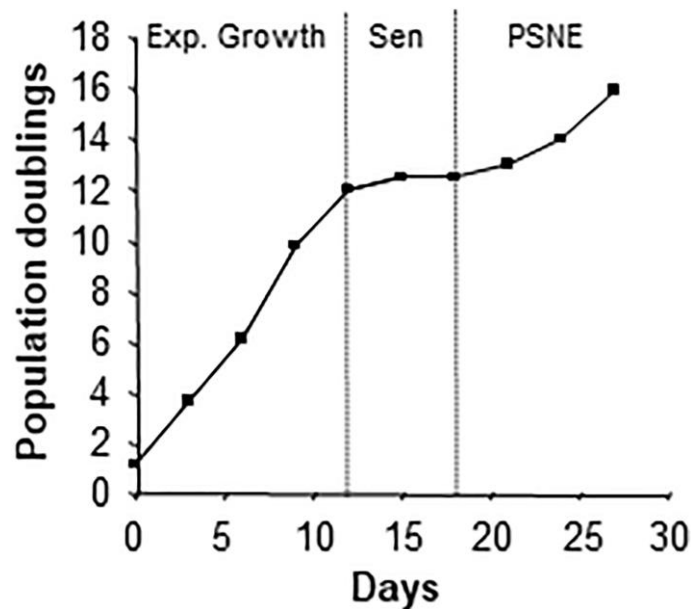
**Supplementary Figure 3: Contribution of ROS-generating activity of PTGS2 to the senescent phenotype in NHEKs.** (A) NHEKs (donor K23FC1) at the exponential growing phase or at the senescence plateau were treated or not with NS398 or rofecoxib for 16 hrs. ROS levels were analyzed by using the H<sub>2</sub>DCFDA probe. The fluorescence was normalized to cell numbers and was expressed as relative values, a value of 1 corresponding to the level of fluorescence in exponentially growing cells. (B) Senescent NHEKs (donor K23FC1) were transfected with a pool of 4 siRNAs targeting PTGS2, or with non-target siRNAs. ROS levels were measured and analyzed as in (A). In A and B, the measures were performed in triplicate. The bars represent the mean + SD.



**Supplementary Figure 4. Evaluation of PTGES1 and PGFS silencing efficiency.** (A) Analysis of PTGES1 protein levels in senescent NHEKs (Donor K40FH1) subjected to PTGES1 silencing compared to a non-target siRNA as control 96h after transfection. GAPDH was used as loading control. (B) Analysis of the amount of PGF2α. by competitive assay in senescent NHEKs (Donor K40FH1) subjected to PGFS silencing compared to a non-target siRNA as control 96 h after transfection. The results were normalized to the number of senescent NHEKs. Bars represent the mean ± SD of three independent experiments.



**Supplementary Figure 5. PTGES1 controls the secretion of IL-10 through the production of PGE<sub>2</sub>.** Senescent NHEKs (Donor K40FH1) were transfected with a pool of 4 siRNAs targeting PTGES1, or with non-target siRNAs (siCtrl). Two days after transfection, NHEKs were treated or not with 1 µM PGE<sub>2</sub> 4-times a day during 3 days. The amounts of IL-10 in the conditioned media (secreted) were measured by an ELISA assay. Measures were performed in triplicate. Bars represent the mean +/- SD. Significant differences are indicated with asterisks with \**p* < 0.05 and \*\**p* < 0.01.



**Supplementary Figure 6. Outcome of NHEKs.** NHEK growth curve (from donor 4F0315) showing the exponentially growing, senescent and emergent (PSNE) phases.

## Supplementary Table

Supplementary Table 1. Characteristics of donors of skin samples.

	<b>N° = Patient</b>	<b>Age</b>	<b>Fitzpatrick type</b>	<b>Localization</b>	<b>Smoking</b>
Young	1	39	3	Right arm	no
	29	20	2	Right thigh	no
	46	19	3	Left hip	no
	58	39	3	Right thigh	yes
	4	70	2	Right thigh	yes
Aged	5	82	1	Left inner thigh	no
	9	87	3	Posterior right thigh	no
	55	63	3	Inner side of left knee	no
	56	79	5	Right buttock	no